Cement and Concrete Composites 135 (2023) 104829

Contents lists available at ScienceDirect

Cement and Concrete Composites

journal homepage: www.elsevier.com/locate/cemconcomp

Effect of accelerated aging and silica fume addition on the mechanical and microstructural properties of hybrid textile waste-flax fabric-reinforced cement composites

Payam Sadrolodabaee [a], Josep Claramunt [b], Monica Ardanuy [c], Albert de la Fuente [a,*]

[a] Department of Civil and Environmental Engineering- Universitat Politècnica de Catalunya (BarcelonaTECH)- Barcelona, Spain
[b] Department of Agri-Food Engineering and Biotechnology- Universitat Politècnica de Catalunya (BarcelonaTECH)- Barcelona, Spain
[c] Department of Material Science and Engineering - Universitat Politècnica de Catalunya (BarcelonaTECH)-Barcelona, Spain

ARTICLE INFO

Keywords:
Flax fibers
Freeze-thaw cycles
Textile waste fibers
Supplementary cementitious materials
Textile-reinforced cement composites
Wet-dry cycles

ABSTRACT

Incorporating eco-friendly substances obtained from recycled resources and industrial by-products is gaining increased acceptance among building materials. In this context, a cementitious matrix containing supplementary cementitious materials (SCMs) reinforced by recycled fibers may be a promising solution from both a durability and sustainability perspective. This study presents an extensive experimental program carried out on a cement-based composite with Silica Fume (SF), reinforced with recycled textile waste (TW) nonwoven fabric. Initially, the mechanical strength (compression and flexure) of the Portland cement paste substituted with variable SF content (0%–30%) was characterized. Based on the results, laminate plates having six TW fabric layers impregnated with three different cement pastes −0%, 15%, and 30% SF− were produced, and both the mechanical (flexural and direct tension) and durability (against wet-dry and freeze-thaw cycles) properties of the composite were assessed through testing. Experimental microstructural techniques including thermogravimetric analysis (TGA), X-ray diffraction (XRD), scanning and backscattered scanning electron microscopy (SEM and BSEM) were also used to complement the analysis of the mechanical characterization. The results suggested that the composite modified by 30% SF could protect fibers from embrittlement, thereby offering the greatest durability by increasing flexural and tensile resistances by up to 45% and 55%, respectively, as compared to the sample without SF in the wet-dry cycles. Indeed, the treated composite with 30% SF had almost equal performance in both unaged and aged conditions, showing a flexural strength in the range of 14.5–15.5 MPa and flexural toughness of 8.0–8.7 kJ/m^2, suitable for the targeted applications including ventilated façades. The results and outcomes of this study may serve as the basis for future research on these composites and their potential use in structural applications in the building construction and housing industries.

1. Introduction

Fiber-reinforced concrete and mortar composed of a cementitious matrix and a reinforcement system in different forms may be used in a wide range of structural and non-structural applications. However, sustainability is an issue to be addressed in any potential application and function. Recyclability and CO_2 emissions are considered to be some of the main indicators of environmental sustainability in fiber/textile reinforced mortars (FRM/TRM) [1,2]. To develop more sustainable cementitious building materials, waste and recycled sources, as well as low carbon-embodied materials, are currently being used [3–6]. According to previous studies carried out by the authors [7–9], recycled textile waste (TW) fibers from clothing waste mixed with vegetable fibers (65% and 35% in mass, respectively) are technically feasible to be used as internal reinforcement (in both short or fabric forms) in cement-based matrices to enhance the toughness and post-cracking behavior for non-structural or low-medium performance structural applications. However, the durability of this type of composites, especially in wet-dry cycles, should be studied in greater detail, given the well-known problem of durability of cement-based composites reinforced with vegetable fibers [8,10]. Partial weight replacement of Portland cement (PC) matrix with SCMs (supplementary cementitious

* Corresponding author.
E-mail addresses: payam.sadrolodabaee@upc.edu (P. Sadrolodabaee), josep.claramunt@upc.edu (J. Claramunt), monica.ardanuy@upc.edu (M. Ardanuy), albert.de.la.fuente@upc.edu (A. de la Fuente).

https://doi.org/10.1016/j.cemconcomp.2022.104829
Received 4 March 2022; Received in revised form 13 September 2022; Accepted 24 October 2022
Available online 29 October 2022

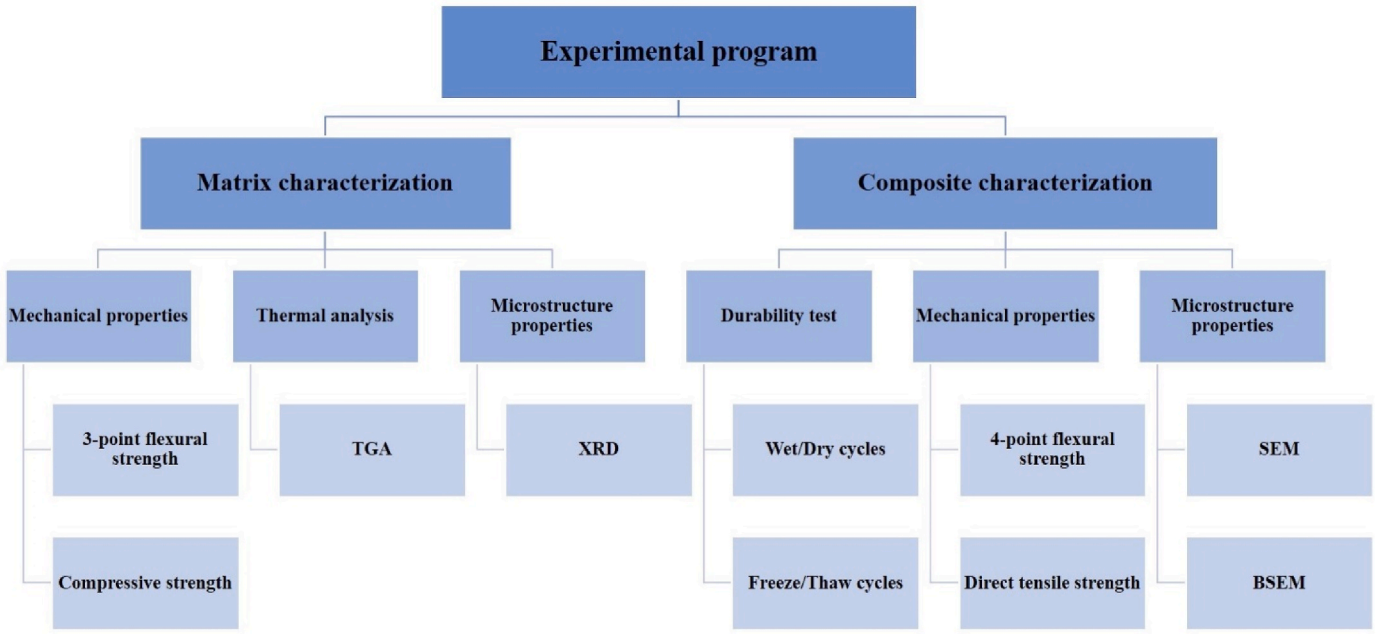

Fig. 1. Schematic of the experimental program of this study.

materials), including pozzolanic and by-products compounds, is a potential solution to address these durability issues, while simultaneously reducing the carbon footprint derived from clinker production (estimated at approximately 5–7% of the global CO_2 emissions).

The lack of durability of composites containing natural fibers is mainly due to the presence of calcium hydroxide, $Ca(OH)_2$, in the PC matrix which degrades the vegetable fibers [11]. To improve durability, certain strategies have been introduced. While some of these strategies modify the fibers through physical and chemical treatments such as hornification [12] or alkaline treatment [13], others modify the matrix to reduce or remove the alkaline compounds, including accelerated carbonation or the use of pozzolanic fillers [14]. The addition of pozzolanic and/or supplementary cementitious materials is intended to transform portlandite (CH) into calcium silicate hydrate (C–S–H) gel. In fact, pozzolanic materials containing a large amount of amorphous silica (SiO_2) and/or alumina (Al_2O_3) promote the pozzolanic reaction during the hydration process, ultimately leading to the replacement of CH by C–S–H [15,16]. Optimized dosages of SCMs to replace cement should be used to ensure the disappearance of portlandite. This optimum dosage is based on matrix composition, curing conditions, and fiber type and content.

According to the literature review, distinct amounts of various SCMs have been used in plant fiber FRM/TRM. Fernández et al. [17] used 10 wt% of sourced silica fume (SF) to achieve a virtual absence of portlandite after autoclaved curing condition in the cement–base reinforced with sisal fibers. Khorami et al. [18] examined the behavior of cement boards reinforced with 8% Kraft pulp waste modified with SF. Their results found that the addition of 3–6% SF by cement weight slightly improved flexural strength, whereas adding more than 6% SF led to a slight reduction of strength as compared to the control specimen. Gutierrez et al. [19] examined the effect of SF, metakaolin (MK), fly ash (FA), and ground granulated blast-furnace slag (GGBS) on cement mortars reinforced with different types of natural and synthetic fibers in the proportion of 2.5% by cement weight. They concluded that the addition of 15% SF or MK improved the composite's performance whereas 15% FA had an adverse effect, probably due to its lower degree of pozzolanic activity. Moreover, they reported that the addition of 70% GGBS offered promising results. Silva et al. [20] managed to improve the durability of the Portland cementitious matrix by incorporating 30% MK and 20% calcined waste crushed clay brick to manufacture composite laminates reinforced with long sisal fibers. Fidelis et al. [21] and Majstorović et al. [22] developed a CH-free matrix by replacing almost 50% of the PC with MK in jute textile-reinforced concrete and flax textile-reinforced composites, respectively.

Other studies have suggested that using SF in the range of 5–45% by cement weight could minimize the loss of toughness of the composites exposed to extreme conditions, while simultaneously improving the impermeability and corrosion resistance [23–26]. Toledo Filho et al. [27] studied the long-term durability of cement composites reinforced with sisal and coconut fibers modified by pozzolanic fillers. Their results indicate that the partial replacement of PC by 40% GGBS does not reduce the embrittlement of the fibers with aging, whereas treatment of the matrix by 10% SF was indeed an efficient method. SF consists largely of amorphous (non-crystalline) silicon dioxide, with ultrafine particles (~100 times smaller than cement particles) [28,29]. As a result of its large surface area (~15 times higher than other pozzolanic materials) and high silica content, SF has been categorized as a highly reactive pozzolanic material, making it a very suitable cementitious material [30]. Numerous studies have reported the favorable impacts of using SF as an SCM in mortar/concrete, including the formation of additional tobermorite-like structure C–S–H gel with a lower calcium-to-silica ratio (Ca/Si) [29], lower permeability, improved pore structures, enhanced interfacial transition zone in concrete, etc. [31–37].

To the best of our knowledge, few results are available in the literature regarding the mechanical and durability characterization of PC composites reinforced with nonwoven fabrics made of recycled fibers from the garment industry. In our previous study [9], the flexural behavior of the TW composite was examined and an optimum number of layers (six) was selected. However, comprehensive studies have yet to be carried out on the improvement in durability against wet-dry and freeze-thaw cycles, or the tensile behavior of this material. Therefore, this work aims to develop durable, ductile, and strain-hardening cementitious composites with variable SF content reinforced with TW nonwoven fabric. To this end, the effect of SF content in the range of 0–30% on the mechanical performance and cement mixture microstructure of the PC matrix was initially evaluated through flexural and compressive tests— at 7 and 28 days— in addition to TGA and XRD analyses. Thus, the optimum percentage of the SF was selected for

Table 1
Mix proportions and nomenclature of matrix samples.

Sample	SF0	SF5	SF10	SF15	SF20	SF25	SF30
Cement (g)	2500	2375	2250	2125	2000	1875	1750
SF (g)	0	125	250	375	500	625	750
Water (g)	750	750	750	750	750	750	750
SP (g)	25	25	25	25	35	35	35

composite production. In the next step, the compression-molded laminated composites treated with three distinct SF dosages −the optimum percentage and two reference dosages (0%, 15%, and 30%)−, reinforced with six layers of fabric were produced and tested under the flexural and tensile configuration in different aging conditions −28 curing days, 28 curing days plus 25 wet-dry (WD) or 25 freeze-thaw (FT) accelerating aging cycles−. Finally, SEM and BSEM observations were carried out to determine the structure-properties relationships.

2. Experimental Procedure

The considered experimental program (see Fig. 1) of this study was classified into two main categories and ten sub-categories, which are described in the following sections.

2.1. Materials

Portland cement Type I 52.5 R with a minimum compressive strength of 52.5 MPa at 28 days according to EN 197–1:2011 standard, supplied by Cementos Molins Industrial, S.A. (Spain) was used to produce the mortars. The chemical composition, as well as the physical and mechanical properties of this cement, are reported in Ref. [9]. Densified SF provided by Arciresa S.A.U. (Barcelona, Spain) with minimum 93.5% SiO_2 content and a density of 2.25g/cm^3, was mixed with the matrix as the pozzolanic addition to reduce the alkalinity of the binder. SF was ground prior to mixing to reduce particle size, increase reactivity, and also to break up larger balls and lumps. To improve the fluidity of the matrices and compensate for the adverse impact of SF on the workability of the fresh pastes, a Sika Viscocrete-3425 superplasticizer (SP) based on modified polycarboxylate polymers provided by the Sika S.A.U. (Barcelona, Spain), was used.

The hybrid nonwoven fabric, with 1 mm thickness and an areal weight of 155 g/m^2, was produced from 65% shredded short recycled TW fibers (by Triturats La Canya S.A., Spain) and 35% long flax fibers (Institut Wlokien Naturalnych, Poland) through card clothing and needle-punching process as described in depth in Ref. [38]. Thus, the final fabric, with a tensile rupture load of 4.0 N and elongation of 20% in the machine direction, consisted of approximately 45% cotton, 35% flax, and 20% polyester fibers.

2.2. Matrix preparation and characterization

Six specimens measuring 160 mm × 40 mm × 40 mm per sample were prepared and cured for 7 and 28 days prior to testing under flexure and compression forces. The curing was performed in a humidity chamber with >90% relative humidity (RH) at 20 ± 1 °C. The w/b ratio was fixed at 0.3 for all of the samples and 1%–1.4% SP by binder weight was added to the paste. Table 1 shows the mixed proportions and the designation of the samples based on the SF dosage expressed in percentage of the cement weight.

The mechanical tests, including three-point flexural and compression modes, were performed according to EN 196–1:2005 standard [39]. The span length of the bending test was 100 mm and an INCOTECNIC press equipped with a load cell of 3 KN capacity at a loading rate of 2 mm/min was used. For the compression test carried out on the other halves of the specimens after the bending tests, the same press, equipped with a maximum load cell of 300 kN, was used. The maximum flexural tensile strength (also called the *modulus of rupture* (MOR)) and the compressive strength of the specimens were determined through Equations (1) and (2). Six and twelve specimens per sample were tested for flexure and compression, respectively.

$$MOR_{3p} = \frac{3P_{max}L}{2bh^2} \quad (1)$$

$$f_c = \frac{P_{max}}{bh} \quad (2)$$

Where P_{max} is the maximum associated load recorded, L is the span length, and b and h are the cross-sectional width and thickness, respectively. The results were statistically treated through an analysis of variance (ANOVA) with the Tukey HSD test performed with the help of SAS GLM software [40].

The chemical compositions of the SF0 and SF30 samples were determined using an X-ray diffraction (XRD) analysis at various aging times (7–270 days) with a diffractometer model D8 Advance of Bruker AXS GMBH (Germany). Data were collected in the range 2θ from 5° to 50° at a resolution of 0.02° and a speed of 1 s/0.02°. The main anhydrous cement phases (C_2S, C_3S, C_3A, and C_4AF) are crystalline and therefore, their detection by XRD is possible, whereas the majority of the hydrated material, such as C–S–H, is amorphous or only partially crystalline [41].

Both TGA and derivative thermogravimetric analysis (DTG) are widely used thermal techniques to evaluate the reactivity of pozzolanic addition and its reaction with PC to reduce the CH content [41,42]. In this study, TGA tests were performed on all cement matrices with a thermobalance TGA-SDTA 851e/SF/1100 from Mettler Toledo. Samples containing approximately 20 mg were heated in an open alumina crucible from 25 °C to 950 °C at 10 °C/min with a flux of nitrogen of 50 ml/min. The percentage of CH in each mixture was calculated from the decomposition of portlandite through Equation (3) as previously stated by other authors [22,43]:

$$CH\ \% = \frac{M_1 - M_2}{M_i} \times \frac{74}{18} \quad (3)$$

Where M_1 and M_2 are the mass of the samples at the start and end of CH decomposition, respectively. M_i represents the initial mass of the sample used in TGA.

2.3. Composite preparation and characterization

The textile-reinforced composite plates were produced based on the hand lay-up and the dewatering techniques (vacuuming and compression), as described in detail in previous works [9,44,45]. To summarize, each sample was produced with six layers of nonwoven fabrics, which led to a fiber weight fraction of 5%, immersed in matrix paste and stacked as a laminated plate in a drilled mold subjected to vacuum. Then, the sample was pressed under 3.3 MPa and unmolded after 24 h. Curing was carried out for 28 days at >90% RH and 20 ± 1 °C, resulting in a laminated plate with a thickness of approximately 10 mm and a surface mass of 16.6 kg/m^3. For the durability tests, the plates were subjected to the accelerated aging process after the 28-day curing, including 25 WD or 25 FT cycles performed in a CCI automatic climatic chamber (CCI Calidad, Spain), according to EN 12467 standard [46]. Each WD cycle started with an 18-h immersion of the specimens in water at 20 °C, followed by a 6-h drying at 60 °C at 60% RH. Each FT cycle extended over 6 h, in which the temperature was changed between −20 °C to +20 °C.

Based on the analyses of the matrices, composites with three different SF mixtures (0%, 15%, and 30%) were produced. The initial w/b ratio was fixed at 1.0, while the final ratio depended on the dewatering technique. For each sample, two plates (300 mm × 300 mm × 10 mm) were produced for flexural and tensile tests. From each of these, six

Table 2
Mix proportions and nomenclature of TW composite plates.

Sample	C0	C15	C30	C0WD	C15WD	C30WD	C0FT	C15FT	C30FT
Cement (gr)	1500	1275	1050	1500	1275	1050	1500	1275	1050
SF (gr)	0	225	450	0	225	450	0	225	450
Water (gr)	1500	1500	1500	1500	1500	1500	1500	1500	1500
SP (gr)	0	15	15	0	15	15	0	15	15
(w/b) $_{final}$	0.45	0.55	0.55	0.45	0.50	0.40	0.55	0.55	0.55

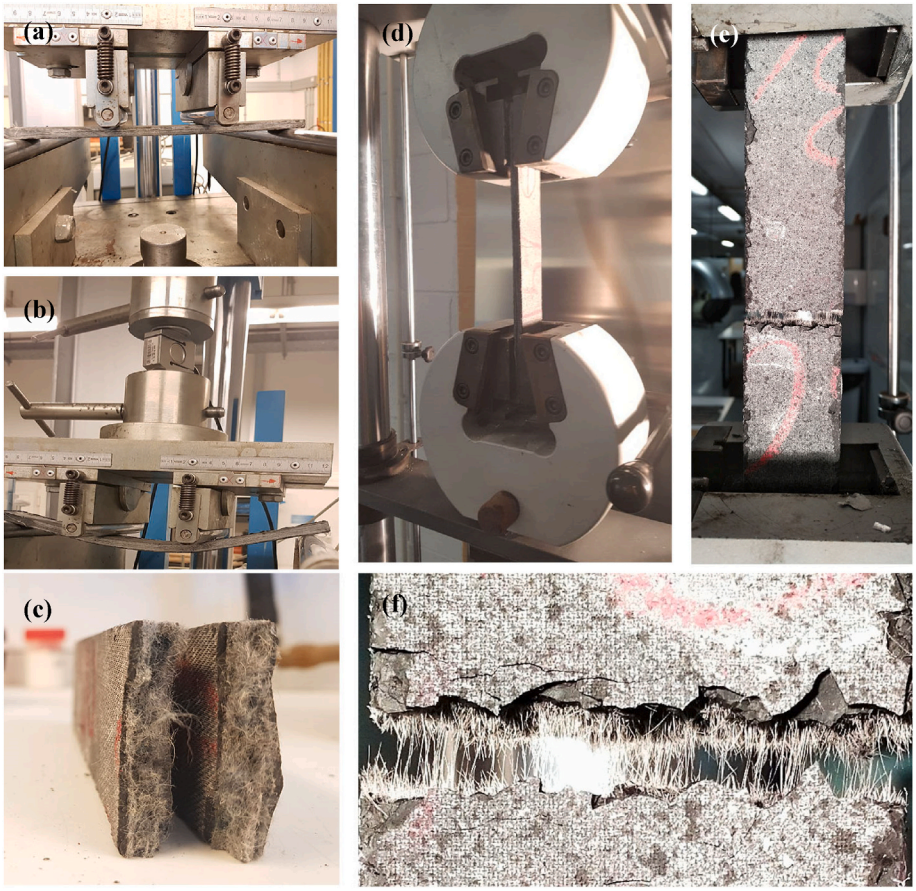

Fig. 2. Mechanical tests on the composites: (a) flexural test set-up; (b) specimens under flexural loading; (c) flexural failure surface; (d) tensile test set-up; (e) rupture of the specimen under tension; (f) tensile failure surface.

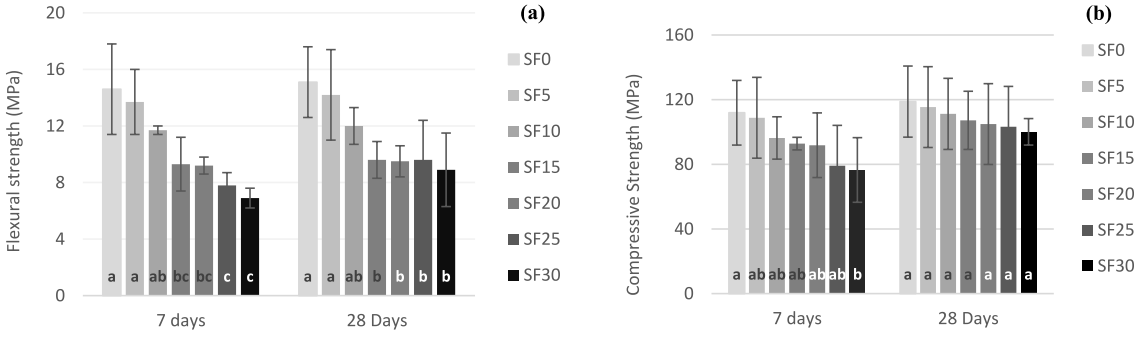

Fig. 3. Mechanical results of the matrix and Tukey HSD test grouping: (a) flexural strength; (b) compressive strength.

specimens were machined (≈300 mm × 50 mm × 10 mm). Table 2 indicates the sample proportions and the composite nomenclature. The number after C reveals the percentage of SF, while WD and FT refer to durability tests: wet-dry and freeze-thaw cycles, respectively.

The mechanical properties of the composites were determined under a four-point flexural test (Fig. 2a–c), following RILEM TFR 1 and TFR 4

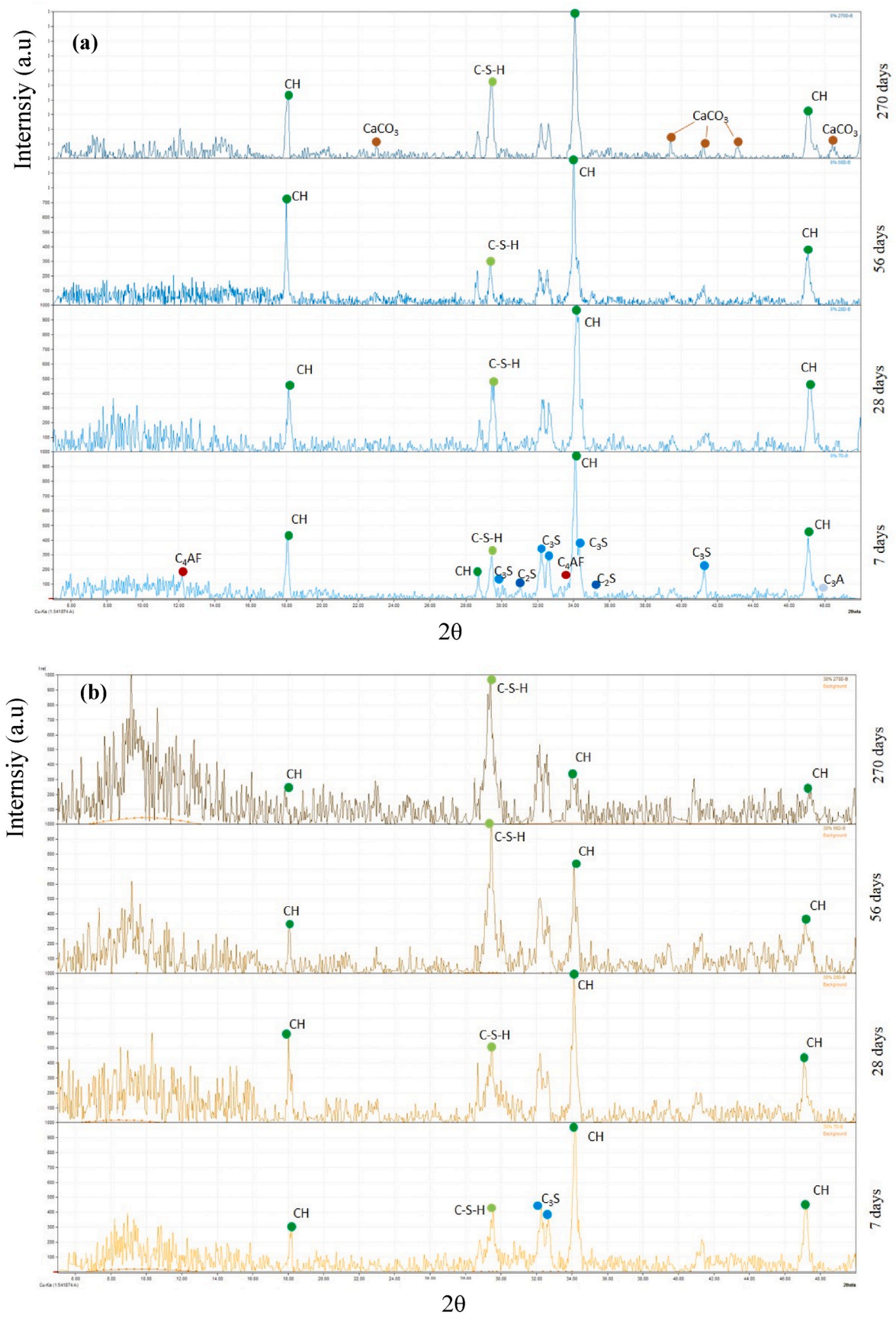

Fig. 4. XRD spectra for matrices with distinct SF content at various ages: (a) SF0; (b) SF30.

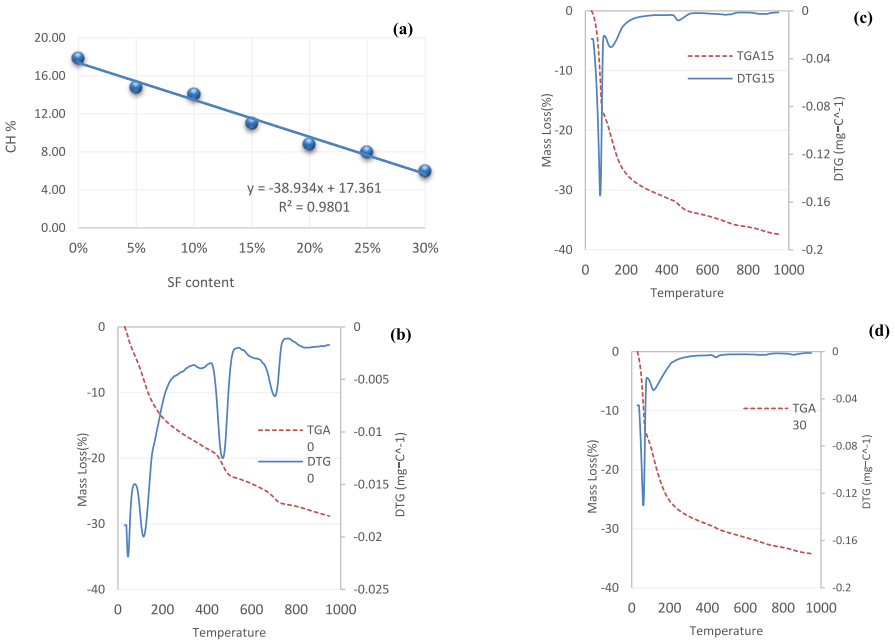

Fig. 5. TGA and DTG results: (a): CH content of all samples; (b) SF0; (c): SF15; (d): SF30.

[47], as well as the uniaxial tensile test (Fig. 2d and e), following RILEM TC 232-TDT [48] with modifications in specimen size. For the flexural test, an Incotecnic universal testing machine (Incotecnic Lab-Pre SL, Spain), equipped with a maximum load cell of 3 kN with a crosshead speed of 20 mm/min and a major span of 270 mm, was used. The following parameters were obtained from this test, as previously described in Refs. [45,49]: the modulus of rupture (MOR) as the maximum flexural stress value through Equation (4); the limit of proportionality (LOP) as the breaking stress value of the matrix (first crack strength); the elastic modulus or the flexural stiffness of the pre-cracked zone (E_{1F}) between 60% and 80% of the LOP from the force-displacement curves through Equation (5); the flexural stiffness of the post-cracking zone (E_{3F}) through the previous formula; and finally, the toughness index (I_{GF}) as the specific fracture energy through the area under the force-displacement curve—limited to a deflection of 10% of the support span—divided by the section of the specimen.

For the direct tensile test, the Metrotec universal testing machine (UTM) from the EETAC SHM/CS2 series (Incotecnic Lab-Pre SL, Spain), equipped with a maximum load cell of 30 kN with a crosshead speed of 10 mm/min and a gauge length of 180 mm, was used. The following parameters were obtained from this test: the ultimate tensile stress (UTS) as the maximum tensile stress value through Equation (6); the bend over point (BOP) as the breaking stress value of the matrix (first crack strength); the tensile moduli as the slope of the stress-strain curve in the pre-cracked zone (E_{1T}) and the post-cracking zone (E_{3T}); and finally, the toughness index (I_{GT}) as explained for the flexural test.

$$MOR_{4p} = \frac{P_{max} L}{bh^2} \tag{4}$$

$$E = \frac{23 \Delta P . L^3}{108 \Delta f . bh^3} \tag{5}$$

$$UTS = \frac{T_{max}}{bh} \tag{6}$$

Where ΔP and Δf are the variations of forces and deflections of two points on the elastic regime or post-cracking regime, T_{max} is the maximum tensile force recorded, and the rest of the parameters are defined according to Equation (1). The main mechanical properties -the maximum resistance and toughness-were statistically treated through the same method as described in the previous section.

Finally, to analyze the microstructure of the composites with a fractured surface, the effects of the accelerated aging cycles as well as the fiber-matrix interface, SEM and BSEM observations were made using a JEOL JSM 6300 (Jeol Ltd., Tokyo, Japan) scanning electron microscope equipped with an energy dispersive X-ray spectrometer (EDS) model Link ISIS-200 (Oxford Instruments, United Kingdom). The hydration reactions of the specimens were frozen by immersion in isopropyl alcohol and specimens were kept under vacuum conditions until analysis. Before BSEM analysis, the specimens were encapsulated in an epoxy resin and polished.

3. Results and discussion

3.1. Mechanical performance of the matrices

The effects of SF content and curing time on the flexural and compressive strengths of the cement matrix are presented in Fig. 3. Further, the associated groups obtained from the ANOVA Tukey HSD test are shown on the charts. As for the evolution of the mechanical properties with curing time, all of the samples in both flexural and compression modes presented a slight increase in resistance at 28 days as compared to 7 days. However, this increased rate was greater for those matrices with more than 15% SF, suggesting that the pozzolanic reaction may proceed more slowly than the reaction of the clinker compounds. In other words, although the control sample and those with low SF content reach the majority of their strength at 7 days, others would continue to gradually increase in strength. This type of later pozzolanic reaction in the almost CH-free mixtures had been previously observed by Toledo Filho et al. [50].

In the bending mode (Fig. 3a), the MOR decreased gradually by increasing the SF content at both 7 and 28 days, as confirmed by the ANOVA analysis –see how the groupings were changing. However, at 28 days, the strength of the SF15 and SF30 samples was almost the same, placed in the same group by the Tukey test, and the difference with the control sample was reduced as compared to 7 days. This suggested that the pozzolanic materials reacted a bit more slowly and that by increasing the curing time, resistance would be increased. Indeed, as reported in

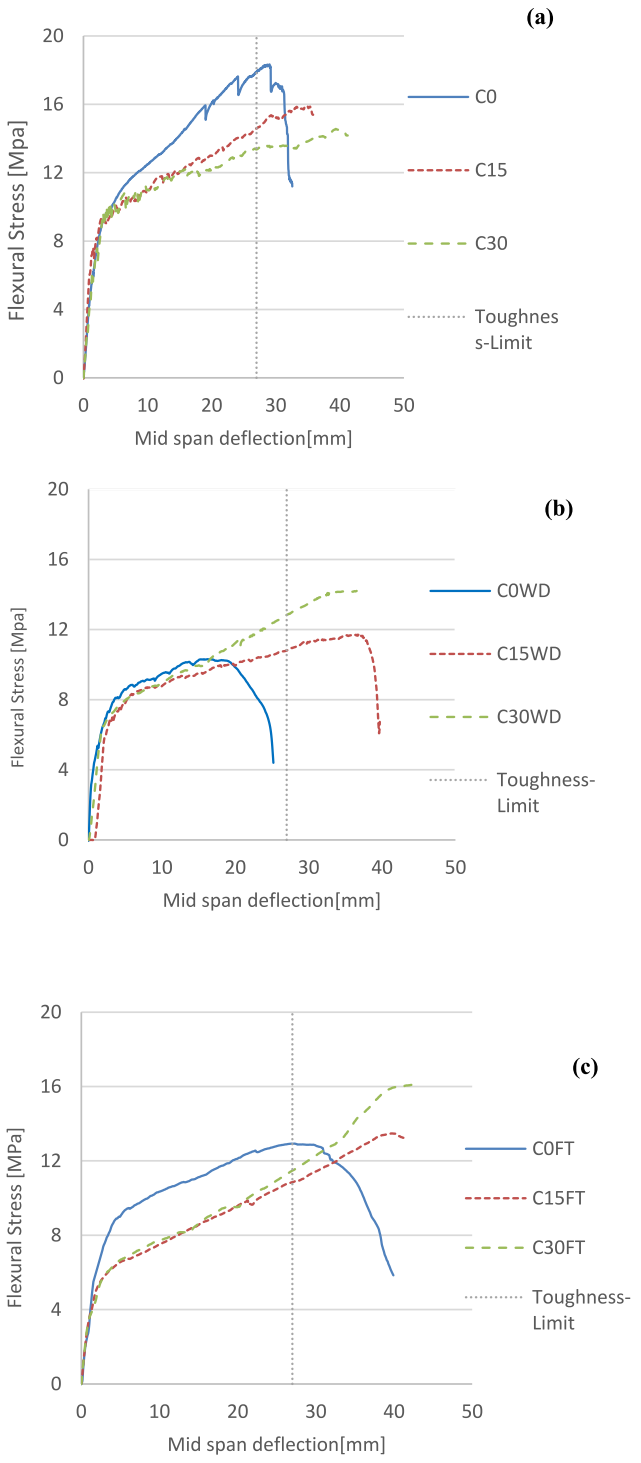

Fig. 6. Experimental flexural stress–deflection relationships of TW nonwoven composites in various conditions: (a) unaged; (b) WD aging; (c) FT aging.

some studies [51], the blended pastes would slowly refine pore structures, resulting in increased strength, although their total porosities were equal or even higher as compared to pure PC pastes. However, in the study of Reamizrez et al. [49], adding distinct dosages of MK to the calcium-aluminate cement matrix led to a reduction of MOR with aging after 28 days. Additional and more detailed research on longer curing times with different matrices is necessary to clarify this behavior.

As for compressive strength (Fig. 3b), the values decreased gradually by increasing the SF amount at 7 days –various groupings were observed by the Tukey test. However, all samples at 28 days reached 100 MPa, placed in the same group by ANOVA, suggesting that matrix hydration is incomplete at early curing time due to the low w/b ratio (0.3) and the slow pozzolanic reaction, maintaining a certain amount of unhydrated particles. These particles can be subsequently hydrated, precipitating in porous regions of the matrix, hence filling the pores and increasing the compressive strength.

3.2. Microstructure of the matrices

Fig. 4 presents the XRD spectra for the matrices of SF0 and SF30 samples at 7 to 270 curing days. As seen at 7 days for both samples, not all of the cement particles were hydrated and, therefore, the process evolved according to aging and degree of hydration, i.e., the anhydrous phases (C_3S, C_2S, C_3A, and C_4AF) were decreasing while the hydrated ones (CH, C–S–H, $CaCO_3$) were increasing from 7 days to 270 days curing. For the SF0 sample at 270 days, the amount of portlandite decreased slightly due to the carbonation process which resulted in calcite formation. For the SF30 sample (see Fig. 4b), the C–S–H wave was intenser due to the reaction of SF with CH. Although up to 28 days, SF0 and SF30 spectra were almost similar, at 56 days the C–S–H had become the major phase in SF30, and specifically at 270 days, the portlandite had virtually disappeared due to the clinker replacement and pozzolanic reaction which advanced slowly. Indeed, for the SF30 sample, the initial increase in CH content lasted up to 28 days after the onset of PC hydration, after which the CH began to decrease due to the pozzolanic reaction triggered by SF. Thus, based on the XRD analysis, the SF30 sample could decrease the alkalinity of the matrix and increase the C–S–H with aging, especially after 56 days.

As for the TGA, in the cementitious matrix, the mass loss up to 600 °C tends to be related to the loss of water and above that temperature, to the release of CO_2 [52]. While Portlandite dehydroxylates mainly in the range of 400°C–550 °C ($Ca(OH)_2 \rightarrow CaO + H_2O$), calcium carbonate ($CaCO_3$) decomposes above 600 °C to CaO and CO_2 [53]. C–S–H phases experience water loss over a wide range of temperatures (specifically 50 °C–400 °C) due to the loss of water in the interlayer and dehydroxylation [42,52].

Fig. 5a shows the amount of CH obtained from TGA and DTG analyses for all the matrices. As seen, the amount of CH decreased almost regularly by increasing the SF, however, the reduction was only significant from the SF15 composite onwards (less than 20% for SF5 and SF10), indicating that 5–10% SF barely decreases the alkalinity of the matrix. Thus, from the SF15 composite onwards, the amount of CH decreased more severely, approximately 38%, reaching its minimum in the SF30 sample, at which point it was reduced by almost 66% with respect to the sample without SF.

Fig. 5b–d shows the TGA curves and the corresponding derivatives (DTG) for the SF0, SF15, and SF30 samples, based on weight loss and the exposed temperature. For the SF0 sample (Fig. 5b), the DTG curve's main peak was observed in the range of 400°C–600 °C, corresponding to the decomposition of CH, which resulted in a water loss of the matrix of almost 45%. A shorter peak was observed between 600 °C and 850 °C, which may be related to the decomposition of calcite and loss of CO_2 [54], as the presence of calcium carbonate was previously confirmed in XRD results. Some other shorter peaks were observed before 400 °C, which can be associated with water loss due to C–S–H decomposition. However, the DTG curves of the SF15 and SF30 samples (Fig. 5c and d) have shown no significant peak in the range of temperature related to CH dehydration, confirming the XRD results showing that the amount of CH was lower as compared to the SF0 sample. The main peaks were observed at less than 200 °C, which may be possibly associated with the water loss due to the C–S–H phase decomposition.

Thus, XRD and TGA analyses revealed that matrices with less than 15% SF presented a high amount of portlandite and were not suitable for improving the durability of the composites although they presented a higher mechanical resistance, especially at 7 days. Matrices with higher

Table 3
Flexural properties (CoV in %) of all samples.

CODE	MOR (N/mm^2)	Tukey test grouping (MOR)	LOP (N/mm^2)	MOR/LOP	I_{GF} (KJ/m^2)	Tukey test grouping (I_{GF})	E_{1F} (GPa)	E_{3F} (GPa)
C0	16.5 (12)	a	6.3 (19)	2.6	10.1 (12)	a	11.3 (21)	0.40 (9)
C15	14.9 (15)	ab	5.5 (20)	2.7	8.9 (18)	ab	11.0 (26)	0.37 (28)
C30	14.5 (13)	ab	5.2 (24)	2.8	8.6 (13)	ab	10.8 (22)	0.38 (24)
C0WD	10.0 (27)	c	6.4 (31)	1.6	6.5 (33)	b	12.0 (5)	0.15 (24)
C15WD	12.5 (10)	bc	5.9 (12)	2.1	7.7 (13)	b	11.2 (12)	0.22 (17)
C30WD	14.3 (3)	ab	5.8 (13)	2.4	8.1 (10)	ab	11.0 (8)	0.30 (14)
C0FT	12.5 (15)	bc	6.5 (21)	1.9	7.4 (16)	b	12.0 (31)	0.27 (30)
C15FT	14.3 (14)	ab	5.9 (22)	2.4	8.2 (20)	ab	11.5 (26)	0.30 (30)
C30FT	15.4 (12)	ab	5.8 (20)	2.7	8.7 (22)	ab	11.1 (22)	0.35 (32)

SF percentages, according to their mechanical results, revealed comparable performance at 28 days. Thus, the 30% SF sample led to the lowest amount of CH and was therefore selected as the optimum treatment for creating laminated composites. Furthermore, composites having 0% and 15% SF have been produced to compare the effect of portlandite quantity on the accelerated aging cycles.

3.3. Flexural performance of the composites

Fig. 6 depicts the representative flexural stress-displacement curves of each composite. Likewise, Table 3 presents the mean and CoV (Coefficient of Variation) of the calculated parameters obtained from the flexural tests. The results shown in Fig. 6 confirm that all unaged and aged TW nonwoven fabric layers presented some extent of flexural hardening behavior under bending configuration, with a high capacity for deformation due to multiple cracking formation (see Fig. 7). The cracking phases of the specimens followed the well-known trend including the pre-cracking zone, the transition or crack propagation zone, and the post-cracking zone [55].

According to the results presented in Table 3 and Fig. 8, the LOP decreased slightly when increasing the SF amount in unaged conditions, from 6.3 N/mm^2 to 5.2 N/mm^2, which is in line with the behavior of the matrices explained in the previous section. Moreover, the LOP value of the composites increased after accelerated aging since this parameter was mainly influenced by matrix strength, hence, the hydration and pozzolanic reaction could further increase said value.

On the other hand, the MOR values presented in Table 3 confirm the flexural-hardening response of all the composites (MOR/LOP >1.0). In this regard, the cracking triggered the effective contribution of the fiber layers, which controlled the crack opening by bearing tensile stresses across the cracks. Fig. 8 shows that in unaged conditions, the MOR value decreased slightly with the addition of SF, although the reinforcement capacity remained constant for all three samples (MOR/LOP ≈ 2.7). This may be due to the reduction of the matrix strength as observed in the LOP values. Nevertheless, in aged conditions, the trend was reversed and the MOR value increased by adding SF both in WD and FT cycles as a result of the pozzolanic additions. Indeed, as observed in the TGA of the matrices, the addition of SF reduced the amount of CH, which in turn, reduced the degradation and embrittlement of the fibers in accelerated aging conditions. Thus, the reinforcement capacity of the fibers was higher when 30% SF was added, as compared to the C0 sample (e.g. in WD cycles: MOR/LOP = 1.6 for C0, while MOR/LOP = 2.4 for C30).

As for the accelerated aging cycles, WD caused significant damage to the fibers as compared to FT (especially in the C0 composite) as will be discussed in SEM/BSEM observations. The MOR value was reduced by 40% and 24% in WD and FT cycles, respectively, for the C0 composite, whereas said reductions represent only 16% and 4% for the C15 composite. The C30 sample showed equal or even higher MOR (in accelerated aging cycles) than the unaged sample as the fibers almost remained undamaged (see the values of E3F in Table 3) whereas the LOP increased. The grouping obtained from ANOVA confirmed this performance as the sample with 30% SF remained in the same group (ab) for all conditions, while the groups of the control sample changed after WD and FT cycles.

The values of toughness (I_{GF}), as a reference parameter for assessing the ductility and energy absorption of the composites, are presented in both Table 3 and Fig. 9. The results reveal that I_{GF} follows a similar trend to that obtained for MOR. That is, the C0 sample had the highest I_{GF} value among the unaged composites whereas in aging conditions, the C30 sample had the highest value. Again, based on the Tukey HSD test, the C30 sample had the same group in all conditions which proved that the energy absorption of the material remained almost constant after accelerated aging. The observed trends for MOR and I_{GF} in this study are in line with other observations in which the effect of SCMs on the WD accelerated aged condition was examined through the flexural test for the vegetable-based fiber reinforced mortar composites [27,49,50]. In all the studies, the MOR and I_{GF} of the unaged composites were slightly reduced after substituting cement with SCMs (10% SF, 10% MK, and 50% MK/calcined waste, respectively). Furthermore, these parameters decreased significantly for the reference samples −without SCMs− when exposed to WD cycles. Nonetheless, the SCMs in all studies could improve those parameters in aging conditions with respect to aged reference samples.

In this study, although WD cycles negatively affected the toughness of the C0 composite and caused a loss of over 35%, this loss was only 5% for the C30 composite, proving that the remaining CH had an almost negligible effect on fiber degradation. Moreover, the adverse effect of FT cycles was considerably less than WD, confirming that the WD cycles are the most critical durability tests for natural-based fibers, as reported in Refs. [10,56]. Fig. 7 reveals that the composites in unaged and FT conditions had a more uniformly distributed multi-cracking pattern (higher number of cracks with less spacing) while following the WD cycles, the samples had fewer and wider cracks. This same cracking pattern was reported by Toledo Filho et al. [50] as to the comparison of unaged with WD cycles of sisal reinforced composites. Indeed, under constant environmental conditions, the transfer of OH^- ions or $Ca2^+$ ions from the cement matrix to the fibers is slow. However, exposure to repeated WD cycles causes the capillary pore system of the cement matrix to be consecutively filled and emptied with alkaline pore water, resulting in a faster transfer of the hydration products to the fibers which, in turn, leads to fiber mineralization and embrittlement [57].

Finally, the flexural stiffness of the pre-cracked (E_{1F}) and post-cracked (E_{3F}) zones (see Table 3 and Figs. 10 and 11) were also calculated from the flexural load–midspan deflection curves. As can be seen, the TW reinforcement is not a governing factor in pre-cracked stiffness ($E_{3F}/E_{1F} \leq 0.04$ in all cases) since the matrix did not crack in this stage. Therefore, the fibers do not effectively contribute to this stiffness. Moreover, E_1 follows almost the same trend as LOP since both parameters are mainly dependent on the matrix characteristics (i.e., after durability tests, the elastic pre-cracking properties (LOP and E_{1F}) remained constant or increased by up to 5% since these mainly depend on the matrix, rather than on fibers). A similar trend, unaltered or even higher amounts for LOP and E_{1F} after the aging of the cement composites, was observed in other research [58,59].

On the other hand, E_{3F} is governed mainly by the stiffness of the fabrics as the matrix was cracked in the post-cracked regime, and only

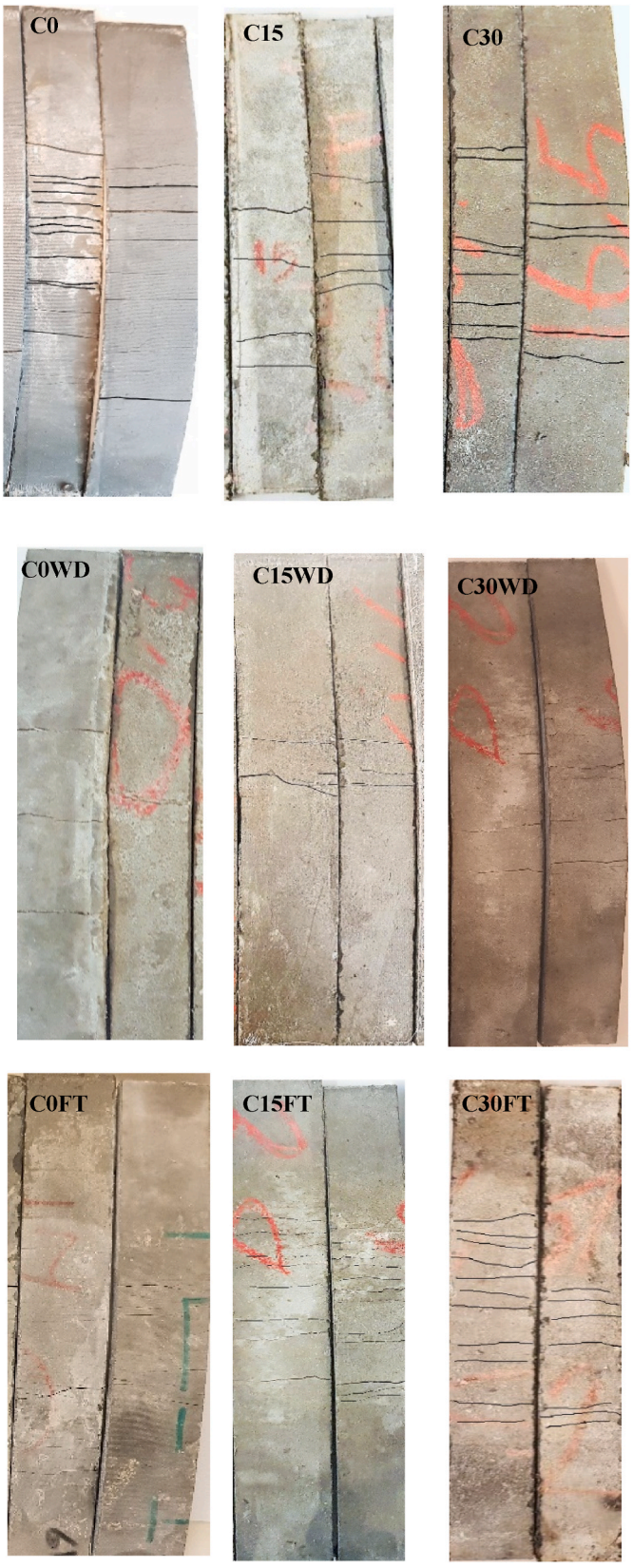

Fig. 7. Typical cracking pattern of the composites after the flexural test.

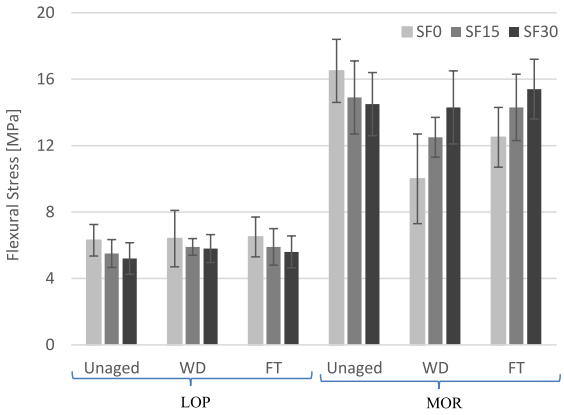

Fig. 8. Flexural strength of the nonwoven composites.

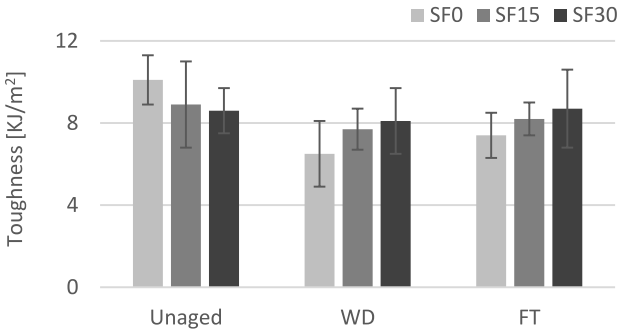

Fig. 9. Flexural toughness (IGF) of the nonwoven composites.

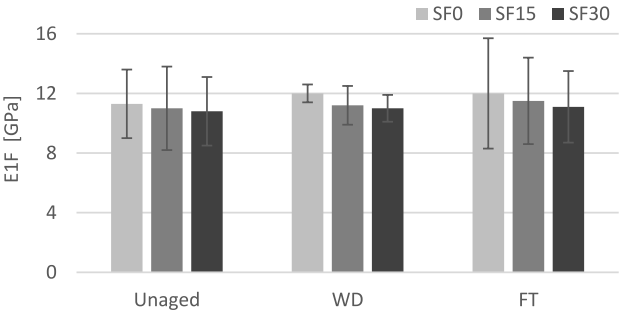

Fig. 10. Flexural stiffness of the pre-cracked zone.

fibers bear the tensile stresses. As can be seen in Fig. 11, WD cycles caused the stiffness of fibers in the C0 composite to degrade significantly (more than 60%) while this amount was half in FT cycles. By adding SF, the degradation of the fibers' stiffness decreased (only 20% and 7% in WD and FT, respectively, for C30) leading to promising results in post-cracking behavior for the C30 sample after aging. Moreover, as seen in Fig. 6b, although the aged composite demonstrated flexural hardening with multiple cracking behavior, the slope of the post-cracked zones (E_{3F}) was lower than the corresponding unaged composites (Fig. 6a), especially as compared to C0 (60%), indicating the loss of the fibers' stiffness due to degradation.

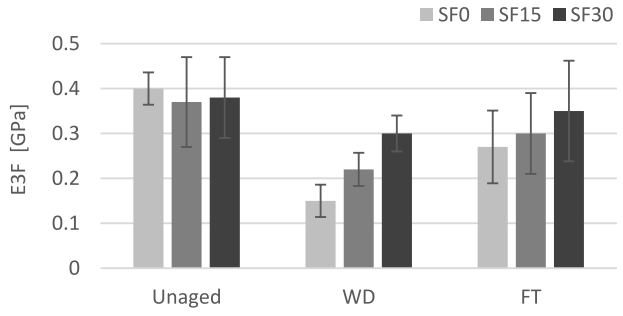

Fig. 11. Flexural stiffness of the post-cracked zone.

3.4. Tensile performance of the composites

Fig. 12 shows the tensile stress-strain curves of the composite samples in both unaged and aged conditions. Likewise, Table 4 presents the mechanical properties obtained from the previous curves. All of the curves in Fig. 12 started with the elastic-linear range, in which both the matrix and the fiber behaved linearly. In this first zone, the stiffness of the composite (E_{1T}) is dominated primarily by matrix properties due to the low volume fraction of fibers and lower fiber stiffness with regard to the matrix (less than 20 times). The second zone (cracking stage) was started by an initial crack formation (BOP value) and propagation in the matrix phase. This is where the fibers start to bridge the cracks and thus, the load-carrying capacity continues by occurring multiple cracking behaviors. Finally, in the third stage, after the crack pattern has completely developed, progressive damage occurred due to the crack widening, which leads to a failure of the specimen by textile rupture or pull-out in the gauge length or textile slippage in the anchored/gripping zones (premature failure since the maximum tensile strength of textile is not achieved) [60]. In this study with the hybrid nonwoven fabric which had very lower tensile strength with respect to the matrix, the first failure mode (main cracks in the middle of the specimen due to fiber pull-out at the fracture section) happened as seen in Fig. 2e and f. Further, the load drops corresponding to the occurrence of cracks were not pronounced (see Fig. 12) which proved the acceptable bond between the reinforcement and mortar.

The results presented in Table 4 and Fig. 13 reveal that the TW fabric was effective in enhancing the post-cracking behavior of the materials (UTS/BOP >1.0). The addition of SF to the composites in unaged conditions had a negligible effect on all of the mechanical properties, see Tukey test grouping for UTS and I_{GT}. However, this pozzolanic material proved its efficiency in aging cycles. While WD and FT cycles reduced the UTS (50% and 30%, respectively) and toughness (80% and 60%, respectively) of the C0 sample (see Fig. 14), the adverse effect of these accelerated aging cycles on the samples containing SF, especially those with 30%, was noticeably inferior. As for the WD cycles, the C15 sample lost 35% and 50% of its resistance and energy absorption, respectively, while for the C30 sample, said reductions represented only 15% and 36%. Regarding FT, the loss was even less significant (10% and 37% for the C15 sample in UTS and I_{GT}), proving that this type of aging is less critical than WD. The C30 sample demonstrated virtually no mechanical loss in post-cracking parameters after the FT cycles, both UTS and I_{GT} remained in the same Tukey test group (a).

The pre-cracking properties including BOP and E_{1T} (see Fig. 15) did not change or even improve slightly with aging since the matrix could be hydrated even more during the aging cycles. The addition of SF to the composite did not have a significant effect on these properties.

As seen in Fig. 16, E_{3T} was reduced by aging, especially for the C0 sample in WD conditions −almost 90%− revealing the stiffness degradation of the fiber due to mineralization and migration of CH to the fiber

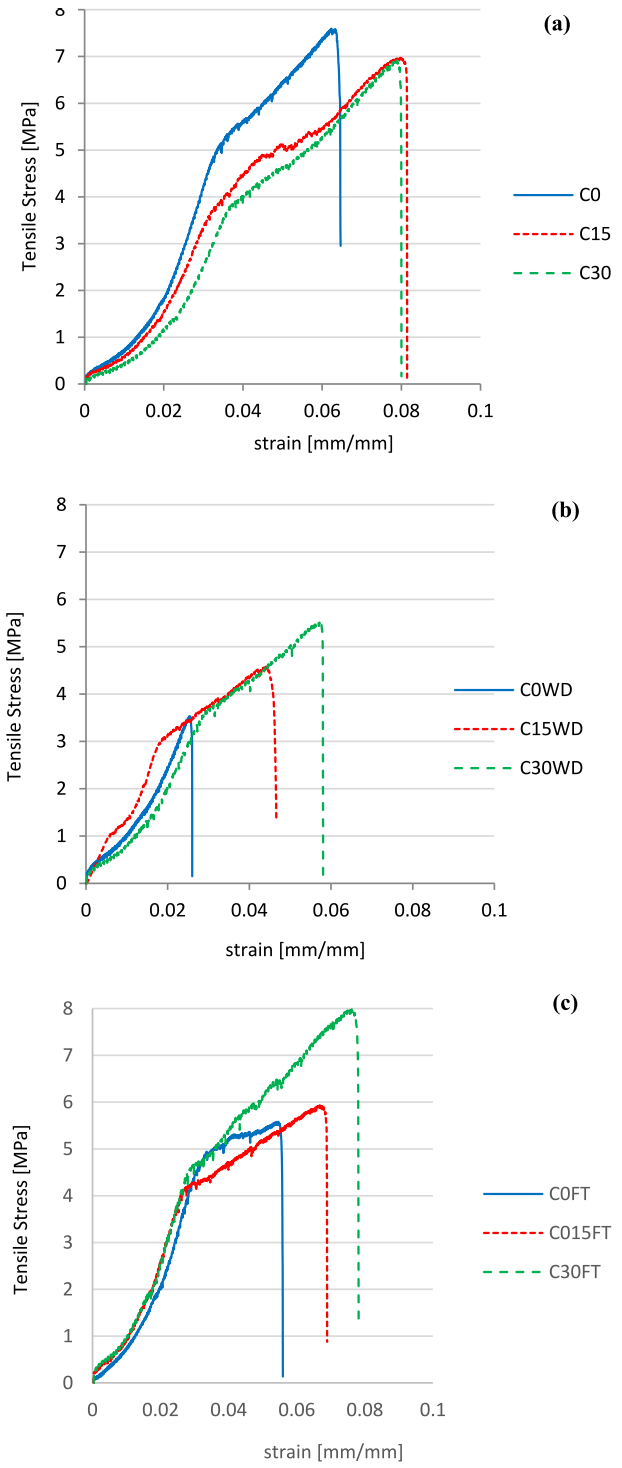

Fig. 12. Experimental tensile stress–deflection relationships of TW nonwoven composites in various conditions: (a) unaged; (b) WD aging; (c) FT aging.

structure. Nevertheless, this loss was less significant for C15 and C30 samples, especially in FT cycles. The C30 composite in FT cycles showed the same mechanical properties as the unaged one since the fiber embrittlement was negligible and the fibers could provide almost the same contribution as in unaged conditions. Indeed, the stiffness of the composite in this stage is associated with the values of the fabric [61].

As for the comparison between the flexural and tensile performance, Fig. 17 shows the amount of ξ for the calculated parameters (e.g. ξ for the maximum resistance will be MOR/UTS) using the C0 composite as a reference since a similar trend was observed for the other samples. The

Table 4
Tensile properties (CoV in %) of all nonwoven composites.

CODE	UTS (N/mm^2)	Tukey test grouping (UTS)	BOP (N/mm^2)	UTS/BOP	I_{GT} (KJ/m^2)	Tukey test grouping (I_{GT})	E_{1T} (GPa)	E_{3T} (GPa)
C0	6.8 (17)	a	3.5 (19)	1.9	45.0 (23)	ab	0.20 (22)	0.086 (9)
C15	6.4 (16)	ab	3.4 (20)	1.8	43.2 (18)	ab	0.14 (20)	0.070 (28)
C30	6.5 (4)	a	3.3 (10)	1.9	50.1 (16)	a	0.15 (22)	0.080 (20)
C0WD	3.5 (18)	d	3.2 (8)	1.1	6.7 (28)	e	0.20 (25)	0.006 (19)
C15WD	4.1 (10)	cd	3.1 (15)	1.3	21.6 (23)	cd	0.17 (22)	0.047 (17)
C30WD	5.5 (5)	abc	3.2 (13)	1.7	32.1 (10)	bc	0.16 (28)	0.055 (24)
C0FT	4.7 (12)	bcd	3.7 (21)	1.2	17.6 (34)	de	0.30 (31)	0.031 (30)
C15FT	5.7 (15)	abc	3.8 (22)	1.5	27.4 (31)	cd	0.20 (26)	0.060 (20)
C30FT	6.9 (28)	a	4.0 (20)	1.7	47.7 (21)	a	0.25 (32)	0.069 (32)

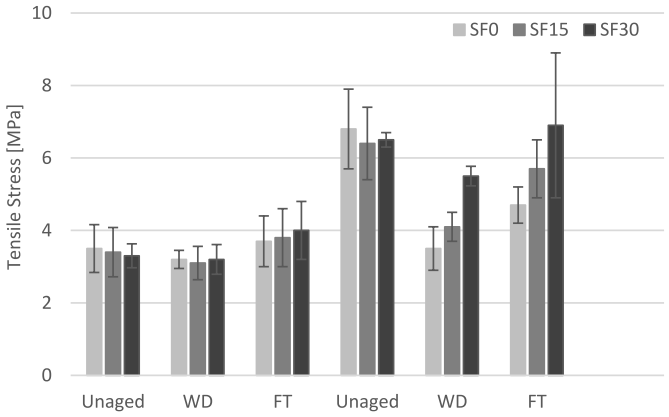

Fig. 13. Tensile resistance of the nonwoven composites.

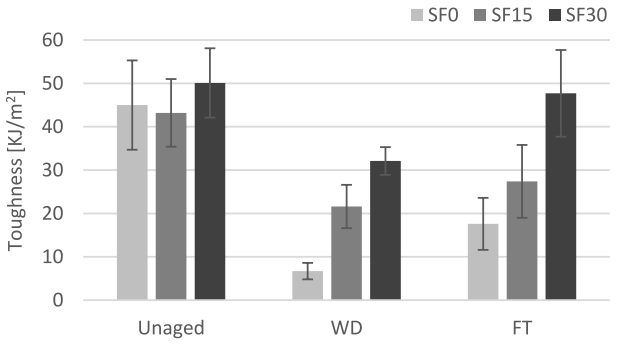

Fig. 14. Tensile toughness (IGT) of the nonwoven composites.

first crack resistance under bending (LOP) occurred on average at stress levels that were 80% higher than those observed for the direct tension test (BOP). A greater discrepancy was noticed for the maximum stresses. Thus, the values reported for MOR are over twice as high as those for UTS. Pre- and post-crack moduli or stiffness were significantly higher for the flexural configuration as well (56.5 and 4.5 times, respectively). The only property that was higher in the tensile configuration was toughness, which was 4.5 times higher in the tensile test. Nonetheless, the general variation trends of all parameters based on aging conditions and SF content were similar in both test configurations. Similar differences between the flexural and tensile resistances were reported in other studies [20,45].

3.5. Microstructure of the composites

Fig. 18 shows the scanning electron micrographs of the breaking

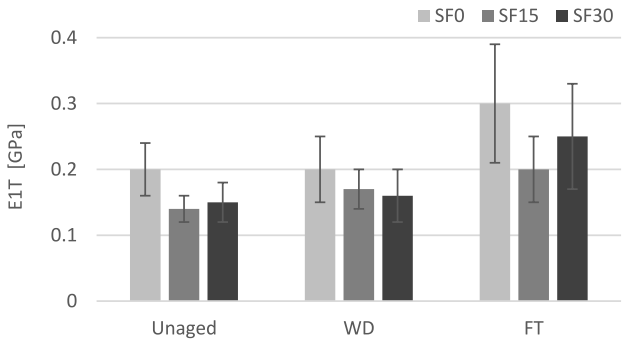

Fig. 15. Tensile stiffness of the pre-cracked zone.

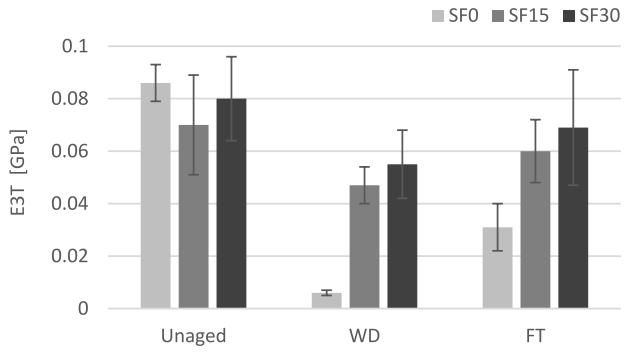

Fig. 16. Tensile stiffness of the post-cracked zone.

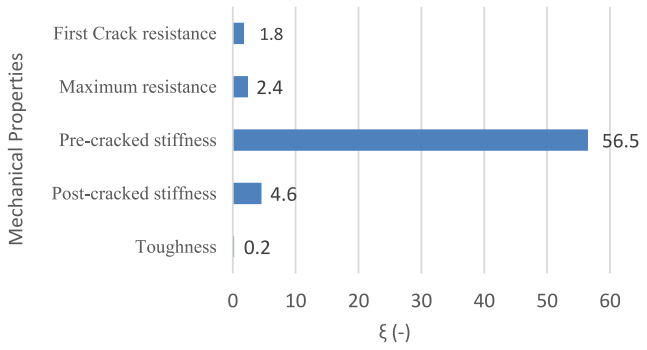

Fig. 17. Comparison between flexural and tensile properties for C0 composite.

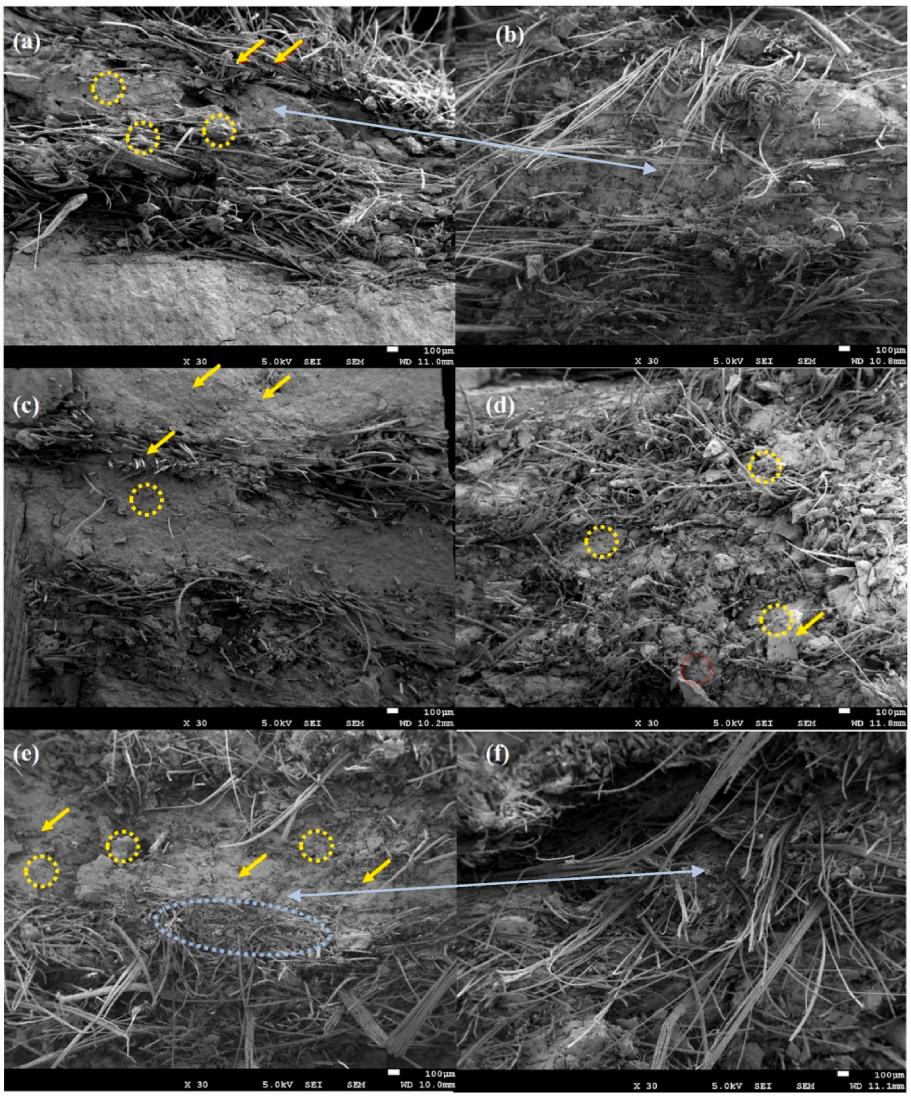

Fig. 18. SEM microimages of the fracture surface of all the composites: (a) C0; (b) C30; (c) C0WD; (d) C30WD; (e) C0FT; (f) C30FT.

section of all composites. The C0 sample had a very flat and clean breaking surface, in which the fibers protrude slightly from the breaking plane. The matrix was slightly disintegrated in the area of the fibers. The fibers were cut close to the breaking section and the pullout holes (yellow dots) can be detected in addition to the fiber rupture cut right at the edge of the section (yellow arrows). In the C0WD sample, the matrix between the fibers was more significantly disintegrated. The fiber rupture, in addition to the fiber pullout, had a smaller length than that of the unaged sample. In the C0FT sample, no significant differences were revealed as compared to the C0 sample. There was similar matrix disintegration with a smaller dimension (dotted blue ellipse) along with the fibers cutting a short distance from the breaking section.

In samples with 30% SF, the extraction of the fiber from the fractured section was longer than the corresponding one without SF. Of these, the C30 and C30FT samples were remarkable due to those points where the reinforcing effect of the fibers was hardly damaged and where the matrix areas were trapped and surrounded by fibers (blue arrows). The C30WD sample showed a disintegrated matrix and the fibers were smaller in length. Nonetheless, the pullout holes of the fibers appeared although it is difficult to find fibers cut right at the edge of the section.

Fig. 19 shows the SEM image of reinforcement in the C0WD sample. Both natural and synthetic fibers broke without elongation, indicating a brittle break, (i.e., the fibers were easily broken at the anchorage section in the mortar). Fig. 19a and b presents the natural cotton fibers where the section revealed concentric fiber layers that were separated from each other by degradation of the hemicelluloses due to the alkalinity of the cement. On the spectra, the deposits in the cotton fibers look like calcium carbonate, derived from the carbonation of calcium hydroxide. Synthetic fibers with a continuous smooth surface can be seen in Fig. 19c and d. The type of breakage is similar to that of cellulose fiber. No significant fiber elongation was observed, which would indicate a sudden break. The image above showed cracks perpendicular to the fiber axis. These cracks could be a consequence of fiber deterioration in the extrusion manufacturing process. Synthetic fibers had fewer deposits and spectra indicate that it may be C–S–H, possibly due to the higher hydrophobicity of synthetic fibers as compared to cotton. In WD cycles, the migration of calcium ions from the matrix to the synthetic fibers most likely occurred less often than in the vegetable fibers due to lower water absorption capacity. In general, the natural fibers were more significantly degraded than synthetic fibers in the C0 sample.

In the sample with 30% SF subjected to WD cycles (see Fig. 20), most of the fibers keep their length after the sample failure, revealing the good tensile strength and flexibility of the fibers. Vegetable fibers with an almost smooth surface had flakes on the surface and some longitudinal cracks, indicating a superficial degradation that was inferior to that of the C0 sample. No main cracks appear as compared to the C0WD

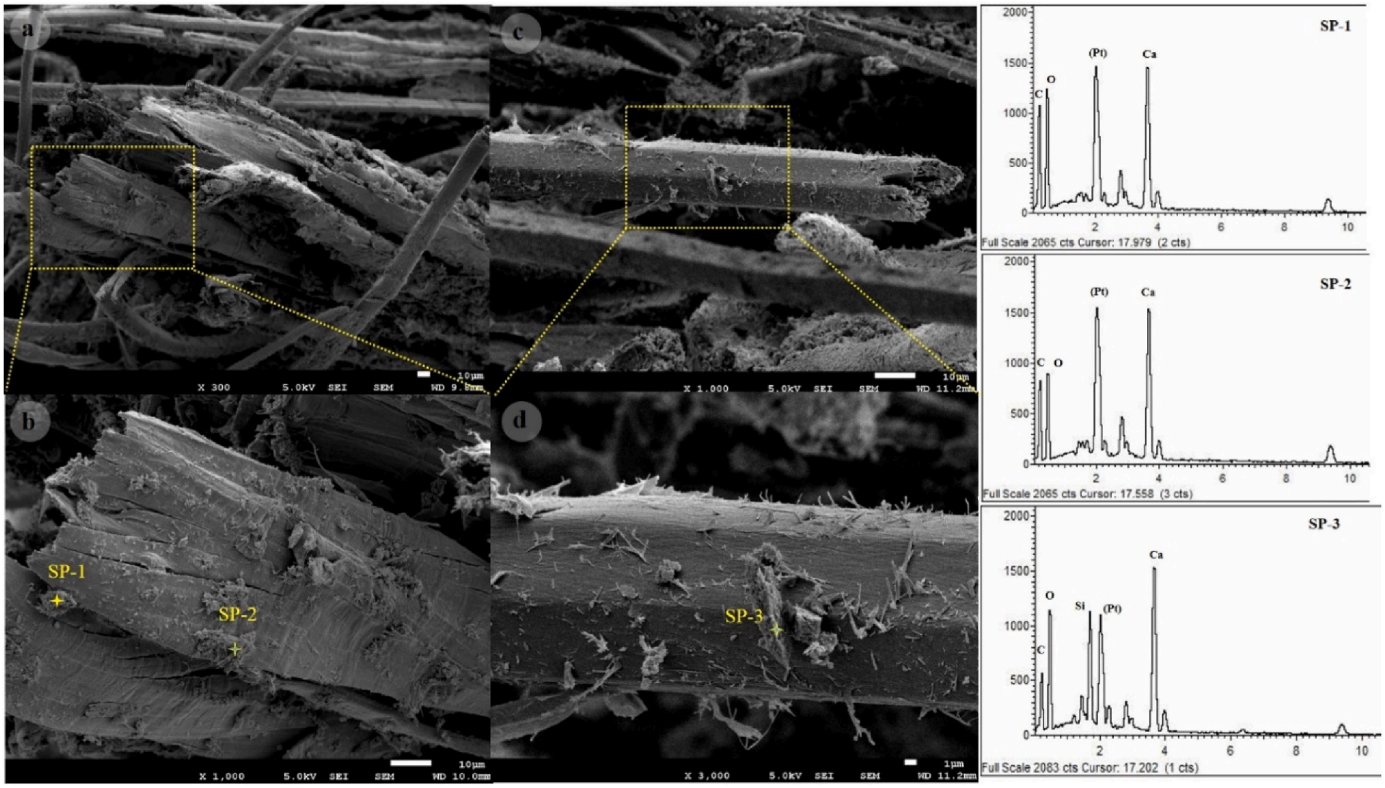

Fig. 19. SEM microimages of the fiber surface in the C0WD sample and the corresponding EDS analysis: (a) vegetable fiber; (b) higher magnification of vegetable fiber; (c) synthetic fiber; (d) higher magnification of synthetic fiber.

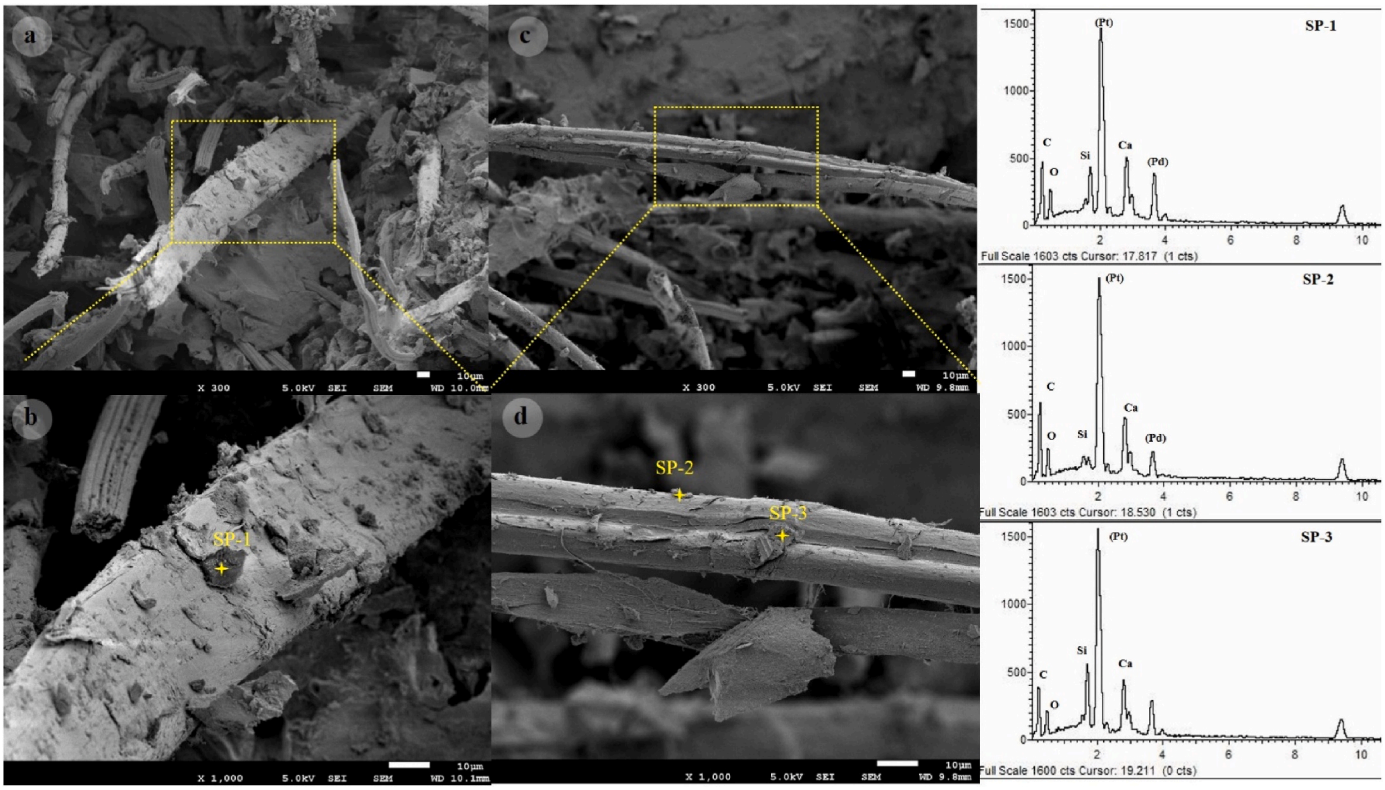

Fig. 20. SEM microimages of the fiber surface in the C30WD sample and the corresponding EDS analysis: (a) vegetable fiber; (b) higher magnification of vegetable fiber; (c) synthetic fiber; (d) higher magnification of synthetic fiber.

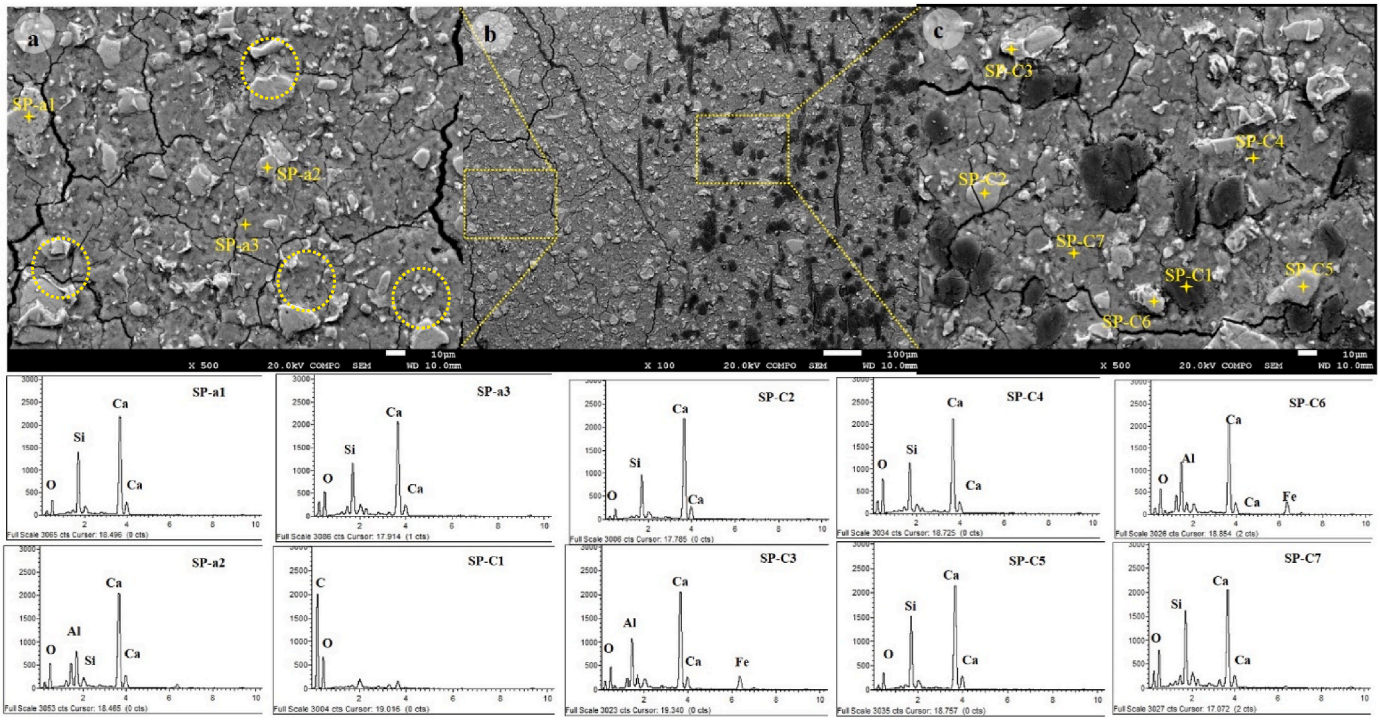

Fig. 21. Backscattered images of the C0 and the corresponding EDS analysis: (a) magnification of matrix area; (b) general image of the composite; (c) magnification of the nonwoven area.

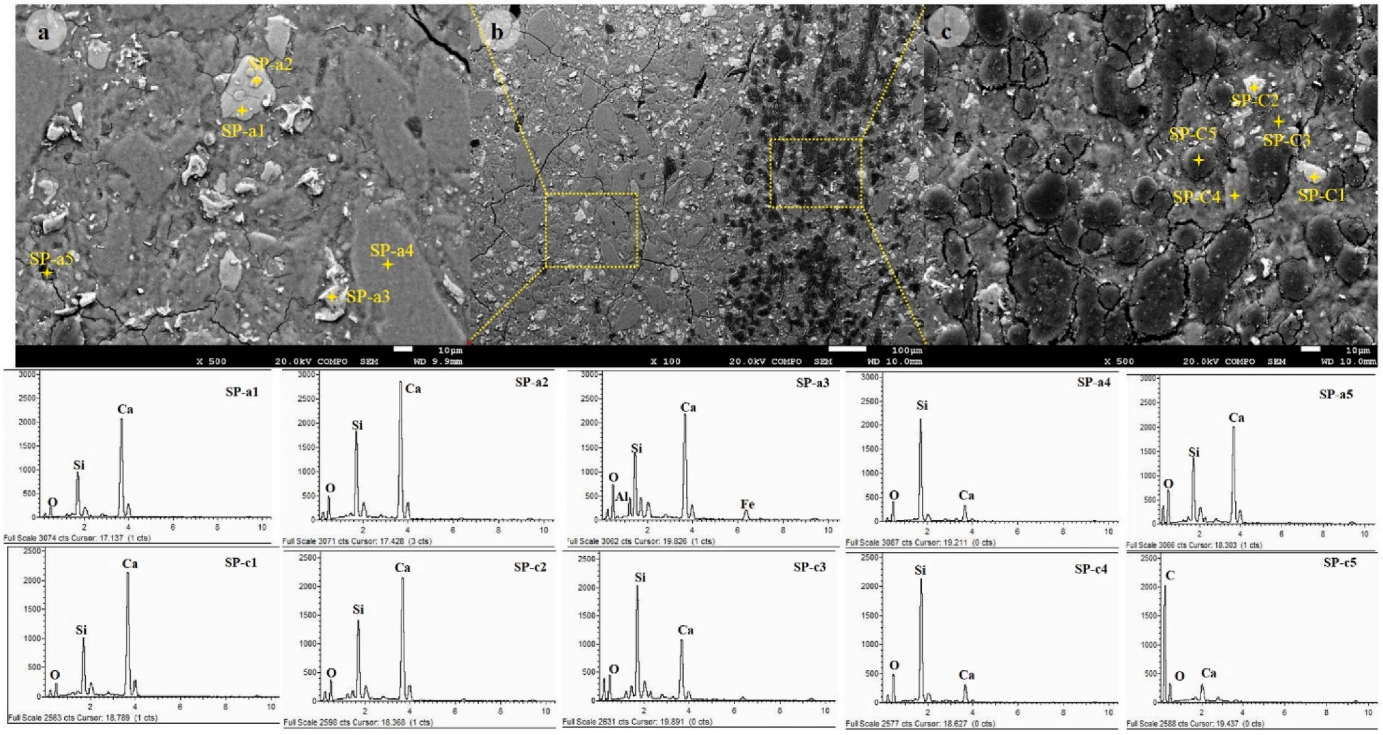

Fig. 22. Backscattered images of the C30 and the corresponding EDS analysis: (a) magnification of matrix area; (b) general image of the composite; (c) magnification of the nonwoven area.

sample, and the fiber did not break at the section edge. Moreover, natural fibers retained a large amount of the cement hydration material on the surface, although clearly grouped in granules. Synthetic fibers, on the other hand, appeared to have less hydrated cement compounds on the surface, possibly indicating a lack of adhesion. Most of these fibers had no serious degradation on their surface, although some minor longitudinal cracks were observed. As for the composition of the compounds adhered to the fibers, the spectra indicated the presence of C–S–H with a few traces of calcium hydroxide associated with the addition of 30% silica fume.

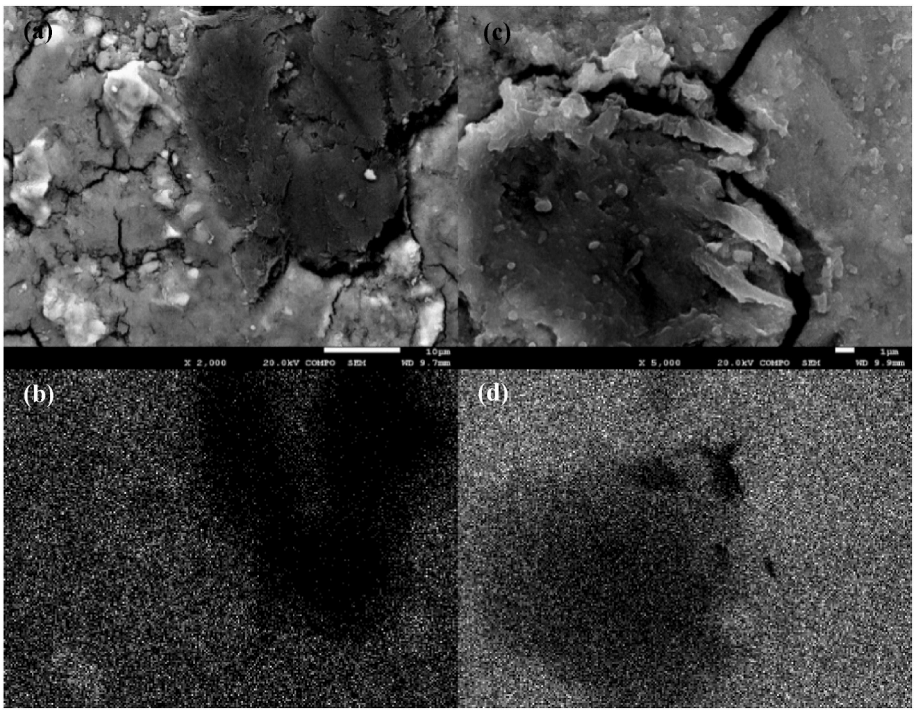

Fig. 23. BSEM images of fiber-matrix interfacial zone and dotting map of Ca ion: (a),(b) C0; (c),(d) C0WD.

Fig. 21 presents a general backscattered image of the C0 composite (Fig. 21b) with two magnifications: the matrix area (Fig. 21a) and the fiber nonwoven area (Fig. 21c). Moreover, the EDS analysis of the selected points to detect the different elements making up the material is also presented. As for the matrix, the anhydrous particles of the cement that have not yet been hydrated can be observed. The spectra indicate the presence of calcium and silicon oxides, most likely allite (C_3S) and bellite (C_2S) in SP-a1. The presence of aluminum, as well as silicon, can be detected in SP-a2. This could be an indication of celite (C_3A) in a polyphase particle, along with allite or bellite. Several anhydrous particles of cement (yellow dots in Fig. 21a) are evident in the matrix zone. In the fiber zone (Fig. 21c) the fibers' ability to absorb and retain moisture generated increased hydration of the cement particles [17]. Thereby, in this area, the anhydrous particles were smaller in size. This phenomenon was most evident around larger diameter fibers, where most particles were less than 1 μm in size. In this case, calcium silicates were detected in SP-c2 and SP-c5, and a ferritic phase (C_4AF), in SP-c3 and SP-c6. As for the hydrated phases, the neutral gray background surrounding the anhydrous particles, amorphous C–S–H was detected in spectra SP-a3, SP-c4, and SP-c7. In SP-c1, carbon corresponding to the fibers was detected. On the other hand, in Fig. 21b the good penetration of the matrix in the structure of the nonwoven was observed, permitting good adhesion to the fibers and ductility.

The main difference between C30 (see Fig. 22) and C0 matrices is the unreacted SF particles. In the area of the fibers, given the higher moisture content generated by the vegetable fibers, there was a greater reaction of the SF particles, leading to the formation of C–S–H (SP-a4 and SP-c4). The same types of anhydrous particles of dicalcium or tricalcium silicates (C_2S and C_3S) were found in SP-a1, SP-a2, SP-c1, and SP-c2. In SP-a3, the presence of silicon, aluminum, calcium, and iron could indicate a polyphasic particle with di-or-tricalcium aluminate fractions, with the presence of C_4AF phases. Moreover, the presence of amorphous areas with calcium and silica with higher oxygen contents indicates that it can be a C–S–H (SP-a5). SP-c3 could indicate an SF particle that has reacted to form C–S–H, given the high presence of Si. Finally, high carbon content in the fibers was observed in SP-c5.

Fig. 23 demonstrates the migration content of the Ca ion from the matrix to the fibers as a result of the WD cycles for the composite without SF. Indeed, due to the WD cycles, CH was dissolved in the water and penetrated the pores and fibers. Fig. 23a shows a fiber surrounded by the matrix of the C0 composite. Around the fiber, some anhydrous particles are observed, along with the hydrated areas. The fiber, dark in color, was well-detected due to its carbon content (low atomic weight). The map of points for the calcium ion of the C0 sample can be seen in Fig. 23b. The fiber was very well-defined and the detection of ions inside the fiber was practically non-existent. Similar details are shown in Fig. 23c–d for the C0WD sample after 25 cycles. The matrix is seen to be fully hydrated as a result of its increased exposure to moisture due to WD cycles. The gap between matrix and fiber is also evident as a result of the fiber hornification causing its shrinkage. Furthermore, the boundaries of the fiber are clearer than its interior. Comparing the center of the fibers in the two different conditions –unaged and aged –, the tone of gray in Fig. 23c is lighter than that of Fig. 23a, indicating the existence of elements with a higher atomic weight. Fig. 23d shows how calcium ions can penetrate and deposit on the fiber after aging. The results confirm the findings of Toledo Filho et al. [57], reporting that the degradation of cellulose fibers is a consequence of the accumulation of Ca-rich phases both in and around the fibers after accelerated aging. Indeed, due to the WD cycles, the matrix quickly lost its moisture whereas the fibers retained it and later became dry, given their absorption and retention ability. This resulted in an increased concentration of Ca ions around the fibers. When the material becomes completely dry, CH precipitates both on and inside the fibers since due to the aging cycles, the pump effect transfers the CH from the matrix zone to the fibers.

Fig. 24 presents the transformation of the matrix after the SF addition and how it affected the fibers after the WD cycles. Fig. 24a is a replica of Fig. 23c which has been incorporated for the purpose of comparing the two composites from samples C0 and C30, after aging. According to Fig. 24c, the area of the matrix in the C30WD sample was almost fully hydrated, as the C0WD one. The fiber has also suffered from shrinkage after the cycles and has been disengaged from the matrix, leaving a certain gap. Fig. 24b,d presents a color mix corresponding to the different ions of aluminum, calcium, silicon, and iron (Al, Ca, Si, and Fe, respectively), which are individually presented below as a map of

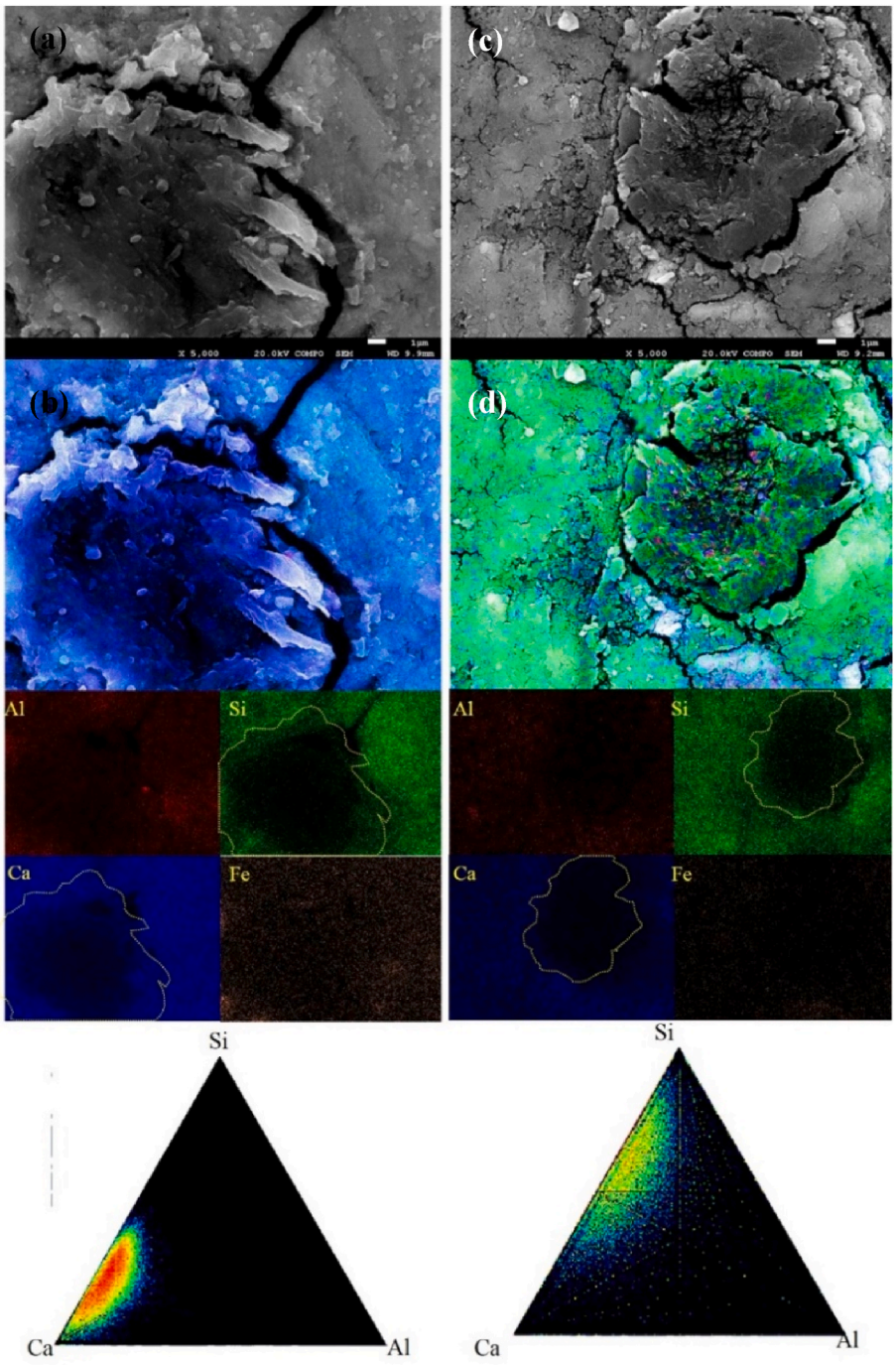

Fig. 24. BSEM images of fiber-matrix interfacial zone and dotting map of chemical element: (a),(b) C0WD; (c),(d) C30WD.

points. As seen for the C0WD sample in Fig. 24b, the concentration of Ca ions was very high with the blue tone predominating in the image. On the other hand, for the C30WD sample, with the incorporation of SF, where the majority of CH transforms into C–S–H, the main ion coloration corresponded to the concentration of Si. Therefore, the final image tone is green. Furthermore, the lower solubility of C–S–H reduces the precipitation of the hydration products in the fibers, thereby avoiding serious mineralization which results in constant reinforcing properties. Finally, the ternary triangular diagrams show the transformation of the matrix from Ca-majority to Si-majority, while maintaining the Al concentration.

4. Conclusions

The main objective of this study was to characterize both design-sensitive mechanical properties (compression, flexure, and direct tension) and durability (against wet-dry and freeze-thaw cycles) of a cement-based −with/without silica fume− textile waste nonwoven fabric reinforcement. The reinforcement is made up of recycled short fibers from the garment industry as well as flax fibers. Cement was replaced by silica fume (SF) by up to 30% to quantify its efficiency in improving the durability of the composite-protection of the fibers.

The following conclusions were made from the experimental program results:

- The study of the matrix suggested that the flexural and compressive resistances decreased with the addition of SF at 7 days of curing. However, at 28 days of curing, the difference between variable samples was reduced, indicating the slow reaction of pozzolanic material. Furthermore, TGA and XRD analyses proved that matrices with less than 15% SF presented a large amount of portlandite and were not suitable for improving the durability of the composites. The lowest amount of calcium hydroxide was found in the C30 sample.
- The results of the flexural tests on the composites showed that wet-dry accelerated aging cycles negatively affected the post-cracking properties of the reinforced composites as compared to the unaged specimens. Nonetheless, composites with 30% SF (C30 sample) presented only slight reductions (<5%) in their mechanical properties as compared to the unaged specimens. The composite without SF (C0 sample) had a resistance 15% higher in unaged conditions than the C30 sample, with a 40% decrease in the wet-dry cycles.
- The results of the direct tensile tests on the composites revealed that the addition of SF had negligible effects on the mechanical properties in unaged conditions. However, composites with SF exhibited better mechanical properties in aged conditions, especially in wet/dry cycles.
- SEM and BSEM observations confirmed that the accelerated aging process, mainly wet-dry cycles, led to an increased fiber fracture ratio and a decreased fiber pull-out strength due to the alkali attack in the C0 sample. Nonetheless, composites containing SF presented a better behavior than the C0 composite, since the amount of calcium hydroxide was significantly reduced (especially in those composites with 30% SF), as confirmed by the TGA study. Thus, the developed PC-based matrix modified with 30% SF prevented fiber embrittlement when submitted to accelerated aging.

Finally, these characterization results of textile waste composites modified with SF allow us to confirm the potential use of this composite as a durable material for building components with limited structural responsibility, offering enhanced sustainability performance. The potential application of this laminated plate as a façade cladding panel has been verified in the Ph.D. thesis of the first author [62].

Declaration of competing interest

The authors declare that they have no known competing financial interests or personal relationships that could have appeared to influence the work reported in this paper.

Data availability

Data will be made available on request.

Acknowledgments

This work was supported through the project grant PID2019-108067RB-I00/AEI/10.13039/501100011033 (RECYBUILDMAT) and PID2019-108978RB-C32/AEI/10.13039/501100011033 (CREEF) by the Ministerio de Ciencia e Innovación (MCIN)/Agencia Estatal de Investigación (AEI) of the Spanish Government.

References

[1] P. Sadrolodabaee, S.M.A. Hosseini, M. Ardunay, J. Claramunt, A. de la Fuente, A New Sustainability Assessment Method for Façade Cladding Panels: A Case Study of Fiber/Textile Reinforced Cement Sheets, Sep. 2021, pp. 809–819.
[2] P. Sadrolodabaee, et al., Experimental characterization of comfort performance parameters and multi-criteria sustainability assessment of recycled textile-reinforced cement facade cladding, J. Clean. Prod. 356 (Jul. 2022), 131900. https://doi.org/10.1016/j.jclepro.2022.131900.
[3] S. Spadea, I. Farina, A. Carrafiello, F. Fraternali, Recycled nylon fibers as cement mortar reinforcement, Construct. Build. Mater. 80 (Apr. 2015) 200–209.
[4] F. Colangelo, I. Farina, M. Travaglioni, C. Salzano, R. Cioffi, A. Petrillo, Innovative materials in Italy for eco-friendly and sustainable buildings, Materials 14 (8) (2021) 2048. Page 2048, vol. 14, Apr. 2021.
[5] F. Colangelo, A. Forcina, I. Farina, A. Petrillo, Life cycle assessment (LCA) of different kinds of concrete containing waste for sustainable construction, Build 8 (5) (May 2018) 70, 2018, Vol. 8, Page 70.
[6] I. Farina, I. Moccia, C. Salzano, N. Singh, P. Sadrolodabaee, F. Colangelo, Compressive and thermal properties of non-structural lightweight concrete containing industrial byproduct aggregates, Materials 15 (11) (2022) 4029. Page 4029, vol. 15, Jun. 2022, https://doi.org/10.3390/ma15114029.
[7] P. Sadrolodabaee, J. Claramunt Blanes, M. Ardanuy Raso, A. de la Fuente Antequera, Preliminary study on new micro textile waste fiber reinforced cement composite, in: ICBBM 2021 4th Int. Conf. Bio-based Build. Mater. Barcelona, 2021, pp. 37–42. Catalunya June 16-18, 2021 Proc.
[8] P. Sadrolodabaee, J. Claramunt, M. Ardanuy, A. de la Fuente, Mechanical and durability characterization of a new textile waste micro-fiber reinforced cement composite for building applications, Case Stud. Constr. Mater. 14 (Jun. 2021), e00492. https://doi.org/10.1016/j.cscm.2021.e00492.
[9] P. Sadrolodabaee, J. Claramunt, M. Ardanuy, A. de la Fuente, Characterization of a textile waste nonwoven fabric reinforced cement composite for non-structural building components, Construct. Build. Mater. 276 (Mar. 2021), 122179. https://doi.org/10.1016/j.conbuildmat.2020.122179.
[10] J. Claramunt, M. Ardanuy, J.A. García-Hortal, R.D.T. Filho, The hornification of vegetable fibers to improve the durability of cement mortar composites, Cem. Concr. Compos. 33 (5) (2011) 586–595.
[11] M. Ardanuy, J. Claramunt, R.D. Toledo Filho, Cellulosic fiber reinforced cement-based composites: a review of recent research, Construct. Build. Mater. 79 (2015) 115–128.
[12] J. Claramunt, M. Ardanuy, J.A. García-Hortal, Effect of drying and rewetting cycles on the structure and physicochemical characteristics of softwood fibres for reinforcement of cementitious composites, Carbohydr. Polym. 79 (1) (2010) 200–205.
[13] B. Koohestani, A.K. Darban, P. Mokhtari, E. Yilmaz, E. Darezereshki, Comparison of different natural fiber treatments: a literature review, Int. J. Environ. Sci. Technol. 16 (1) (Jul. 2018) 629–642, 2018 161.
[14] V. da Costa Correia, S.F. Santos, H. Savastano, Vegetable fiber as reinforcing elements for cement based composite in housing applications – a Brazilian experience, in: MATEC Web Conf, 149, 2018, 01007.
[15] S.F. Santos, G.H.D. Tonoli, J.E.B. Mejia, J. Fiorelli, H. Savastano Jr., Non-conventional cement-based composites reinforced with vegetable fibers: a review of strategies to improve durability, Mater. Construcción 65 (317) (2015) e041.
[16] L. Dvorkin, V. Zhitkovsky, M. Sonebi, V. Marchuk, Y. Stepasiuk, Improving concrete and mortar using modified ash and slag cements, Improv. Concr. Mortar Using Modif. Ash Slag Cem Book- 1st Edition (Apr. 2020). https://doi.org/10.1201/9781003028338.
[17] L. Fernández-Carrasco, J. Claramunt, M. Ardanuy, Autoclaved cellulose fibre reinforced cement: effects of silica fume, Construct. Build. Mater. 66 (September) (2014) 138–145.
[18] M. Khorami, E. Ganjian, The effect of limestone powder, silica fume and fibre content on flexural behaviour of cement composite reinforced by waste Kraft pulp, Construct. Build. Mater. 46 (2013) 142–149.
[19] R.M. de Gutiérrez, L.N. Díaz, S. Delvasto, Effect of pozzolans on the performance of fiber-reinforced mortars, Cem. Concr. Compos. 27 (5) (May 2005) 593–598.
[20] F. de A. Silva, B. Mobasher, R.D.T. Filho, Cracking mechanisms in durable sisal fiber reinforced cement composites, Cem. Concr. Compos. 31 (10) (2009) 721–730.
[21] M.E.A. Fidelis, R.D. Toledo Filho, F. de A. Silva, V. Mechtcherine, M. Butler, S. Hempel, The effect of accelerated aging on the interface of jute textile reinforced concrete, Cem. Concr. Compos. 74 (Nov. 2016) 7–15.
[22] F. Majstorović, V. Sebera, M. Mrak, S. Dolenec, M. Wolf, L. Marrot, Impact of metakaolin on mechanical performance of flax textile-reinforced cement-based composites, Cem. Concr. Compos. 126 (Feb. 2022), 104367.
[23] M. Khorami, E. Ganjian, Comparing flexural behaviour of fibre-cement composites reinforced bagasse: wheat and eucalyptus, Construct. Build. Mater. 25 (9) (2011) 3661–3667.
[24] E. Villar-Cociña, L. Rodier, H. Savastano, M. Lefrán, M.F. Rojas, A comparative study on the pozzolanic activity between bamboo leaves ash and silica fume: kinetic parameters, Waste Biomass Valorization. 11 (4) (Apr. 2020) 1627–1634.
[25] V. Lilkov, I. Rostovsky, O. Petrov, Y. Tzvetanova, P. Savov, Long term study of hardened cement pastes containing silica fume and fly ash, Construct. Build. Mater. 60 (2014) 48–56.
[26] S. Jianxia, Durability design of concrete hydropower structures, Compr. Renew. Energy 6 (Jan. 2012) 377–403.
[27] R.D. Tolèdo Filho, K. Ghavami, G.L. England, K. Scrivener, Development of vegetable fibre-mortar composites of improved durability, Cem. Concr. Compos. 25 (2) (2003) 185–196.
[28] A.I. Nicoara, et al., End-of-Life materials used as supplementary cementitious materials in the concrete industry, Materials 13 (8) (Apr. 2020) 1954, 2020, Vol. 13, Page 1954.
[29] B. Lothenbach, K. Scrivener, R.D. Hooton, Supplementary cementitious materials, Cement Concr. Res. 41 (12) (2011) 1244–1256, Dec.
[30] R. Banar, P. Dashti, A. Zolfagharnasab, A.M. Ramezanianpour, A. A. Ramezanianpour, A comprehensive comparison between using silica fume in the forms of water slurry or blended cement in mortar/concrete, J. Build. Eng. 46 (Apr. 2022), 103802.
[31] A. Mehta, D.K. Ashish, Silica fume and waste glass in cement concrete production: a review, J. Build. Eng. 29 (May 2020), 100888.

[32] M.I. Khan, R. Siddique, Utilization of silica fume in concrete: review of durability properties, Resour. Conserv. Recycl. 57 (Dec. 2011) 30–35.
[33] D. Shen, J. Kang, Y. Jiao, M. Li, C. Li, Effects of different silica fume dosages on early-age behavior and cracking resistance of high strength concrete under restrained condition, Construct. Build. Mater. 263 (Dec. 2020), 120218.
[34] A. Sadrmomtazi, B. Tahmouresi, R.K. Khoshkbijari, Effect of fly ash and silica fume on transition zone, pore structure and permeability of concrete, vol. 70, no. 10, pp. 519–532, https://doi.org/10.1680/jmacr.16.00537, Apr. 2018.
[35] A. Sadrmomtazi, B. Tahmouresi, A. Saradar, Effects of silica fume on mechanical strength and microstructure of basalt fiber reinforced cementitious composites (BFRCC), Construct. Build. Mater. 162 (Feb. 2018) 321–333.
[36] H.G. Mosavinejad, A. Saradar, B. Tahmouresi, Hoop stress-strain in fiber-reinforced cementitious composite thin-walled cylindrical shells, J. Mater. Civ. Eng. 30 (10) (Jul. 2018), 04018258.
[37] A. Saradar, P. Nemati, A.S. Paskiabi, M.M. Moein, H. Moez, E.H. Vishki, Prediction of mechanical properties of lightweight basalt fiber reinforced concrete containing silica fume and fly ash: experimental and numerical assessment, J. Build. Eng. 32 (Nov. 2020), 101732.
[38] H. Ventura, M.D. Álvarez, L. Gonzalez-Lopez, J. Claramunt, M. Ardanuy, Cement composite plates reinforced with nonwoven fabrics from technical textile waste fibres: mechanical and environmental assessment, J. Clean. Prod. 372 (Oct. 2022), 133652.
[39] British Standards Institution., "Methods of Testing Cement. Part 1, Determination of Strength.," p. 33.
[40] SAS: Analytics, Intelligenza Artificiale e Data Management | SAS Italy." .
[41] N.C. Collier, Transition and decomposition temperatures of cement phases - a collection of thermal analysis data, Ceram. - Silikaty 60 (4) (2016) 338–343.
[42] R. Bottom, Thermogravimetric analysis, Princ. Appl. Therm. Anal. (2008) 87–118.
[43] R.D. Toledo Filho, F. de A. Silva, E.M.R. Fairbairn, J. de A.M. Filho, Durability of compression molded sisal fiber reinforced mortar laminates, Construct. Build. Mater. 23 (6) (Jun. 2009) 2409–2420.
[44] J. Claramunt, L. Fernández-Carrasco, H. Ventura, M. Ardanuy, Natural fiber nonwoven reinforced cement composites as sustainable materials for building envelopes, Construct. Build. Mater. 115 (2016) 230–239.
[45] J. Claramunt, H. Ventura, L.J. Fernández-carrasco, M. Ardanuy, Tensile and flexural properties of cement composites reinforced with flax nonwoven fabrics, Materials (2017) 1–12.
[46] BS EN 494-12, Fibre-cement flat sheets - product specification and test methods, Br. Stand. Inst. 60 (2012).
[47] T.C. RILEM, RILEM Recommendations for the Testing and Use of Constructions Materials," CPC 18 Meas. Hardened Concr. Carbonation Depth, 1994, pp. 56–58, 1988.
[48] RILEM Technical Committee 232-TDT (Wolfgang Brameshuber), et al., Recommendation of RILEM TC 232-TDT: test methods and design of textile reinforced concrete: uniaxial tensile test: test method to determine the load bearing behavior of tensile specimens made of textile reinforced concrete, Mater. Struct. Constr. 49 (12) (May 2016) 4923–4927.
[49] M. Ramirez, J. Claramunt, H. Ventura, M. Ardanuy, Evaluation of the mechanical performance and durability of binary blended CAC-MK/natural fiber composites, Construct. Build. Mater. 251 (2019), 118919, https://doi.org/10.1016/j.conbuildmat.2020.118919. In progres.
[50] R.D. Toledo Filho, F. de A. Silva, E.M.R. Fairbairn, J. de A.M. Filho, Durability of compression molded sisal fiber reinforced mortar laminates, Construct. Build. Mater. 23 (6) (Jun. 2009) 2409–2420.
[51] K.O. Kjellsen, E.H. Atlassi, Pore structure of cement silica fume systems: presence of hollow-shell pores, Cement Concr. Res. 29 (1) (Jan. 1999) 133–142.
[52] S. Goto, K. Suenaga, T. Kado, M. Fukuhara, Calcium silicate carbonation products, J. Am. Ceram. Soc. 78 (11) (Nov. 1995) 2867–2872.
[53] Karen Scrivener, Ruben Snellings, Barbara Lothenbach, A practical guide to microstructural analysis of cementitious materials, ISBN 9781138747234, A Pract. Guid. to Microstruct. Anal. Cem. Mater. (Oct. 2018). Book Published by CRC Press.
[54] K.S.P. Karunadasa, C.H. Manoratne, H.M.T.G.A. Pitawala, R.M.G. Rajapakse, Thermal decomposition of calcium carbonate (calcite polymorph) as examined by in-situ high-temperature X-ray powder diffraction, J. Phys. Chem. Solid. 134 (Nov. 2019) 21–28.
[55] M. Saidi, A. Gabor, Iterative analytical modelling of the global behaviour of textile-reinforced cementitious matrix composites subjected to tensile loading, Construct. Build. Mater. 263 (2020), 120130.
[56] M. Ardanuy, J. Claramunt, J.A. García-Hortal, M. Barra, Fiber-matrix interactions in cement mortar composites reinforced with cellulosic fibers, Cellulose 18 (2) (Apr. 2011) 281–289.
[57] R.D. Tolêdo Filho, K. Scrivener, G.L. England, K. Ghavami, Durability of alkali-sensitive sisal and coconut fibres in cement mortar composites, Cem. Concr. Compos. 22 (2) (Apr. 2000) 127–143.
[58] J. Claramunt, L.J. Fernández-Carrasco, H. Ventura, M. Ardanuy, , Natural fiber nonwoven reinforced cement composites as sustainableClaramunt, J. Fernández-Carrasco, L. J, H. Ventura, M. Ardanuy, Natural fiber nonwoven reinforced cement composites as sustainable materials for building envelopes, Constructio," Constr. Build. Mater. 115 (2016) 230–239, 2016.
[59] P. Sadrolodabaee, J. Claramunt, M. Ardanuy, A. de la Fuente, A textile waste fiber-reinforced cement composite: comparison between short random fiber and textile reinforcement, Materials 14 (13) (Jul. 2021) 3742, 2021, Vol. 14, Page 3742, https://doi.org/10.3390/ma14133742.
[60] G. Ferrara, M. Pepe, E. Martinelli, R.D. Tolêdo Filho, Tensile behavior of flax textile reinforced lime-mortar: influence of reinforcement amount and textile impregnation, Cem. Concr. Compos. 119 (May 2021), 103984.
[61] S. De Santis, F.G. Carozzi, G. de Felice, C. Poggi, Test methods for textile reinforced mortar systems, Compos. B Eng. 127 (Oct. 2017) 121–132.
[62] P. Sadrolodabaee, Sustainability, Durability and Mechanical Characterization of a New Recycled Textile-Reinforced Strain-Hardening Cementitious Composite for Building Applications, Doctoral Thesis ,UPC-BarcelonaTECH, 2022 [Online]. Available: https://www.tdx.cat/handle/10803/674796.